



Review Article

Chemical and mineralogical reactions of bentonites in geotechnical barriers at elevated temperatures: review of experimental evidence and modelling progress

Stephan Kaufhold¹ , Reiner Dohrmann^{1,2} , Ilka Wallis³ and Christian Weber¹

¹BGR, Bundesanstalt für Geowissenschaften und Rohstoffe, Hannover, Germany; ²LBEG, State Authority of Mining, Energy and Geology, Hannover, Germany and ³College of Science and Engineering, Flinders University, Adelaide, Australia

Abstract

Bentonites are proposed to be used as buffers in high-level radioactive waste repositories. The elevated temperatures in repositories may, however, affect bentonites' desired properties. For instance, heating under dry conditions can cause cation fixation, potentially affecting swelling properties. The kinetics of mineral dissolution and precipitation reactions will equally be influenced by temperature. Redistributions of Ca-sulphates and -carbonates have been observed, as well as illitization of smectite. Illitization, however, has only been observed in laboratory experiments at large solution/solid ratios, whereas it has not yet been unambiguously identified in large-scale experiments. In many large-scale tests, cation exchange is the first observable geochemical reaction. In addition, an enrichment of Mg close to the heater is found in many such tests. The thermal gradient and (incongruent) smectite dissolution are suspected to play a role with respect to the Mg enrichment, but the underlying mechanism has not been unravelled so far. To predict the long-term performance of a bentonite buffer, numerical modelling is required in order to be able to simulate the reactions of all accompanying mineral phases. Smectites, which dominate the bentonite composition, are therefore particularly difficult to characterise, as their dissolution is often observed to be non-stoichiometric. Various model approaches exist to simulate smectite reactions, mostly based on kinetic rate reactions, ideally considering the effect of pH (congruent or incongruent dissolution), temperature and the degree of saturation of the solution. Reassessing and improving the thermodynamic/kinetic data of smectites are prerequisites for improving long-term buffer performance assessment.

Keywords: Alteration, bentonite, HLRW, modelling, thermal reaction

(Received 12 December 2022; revised 31 August 2023; Accepted Manuscript online: 11 September 2023; Associate Editor: Arkadiusz Derkowski)

Bentonites can be used in repositories for high-level radioactive waste (Neretnieks, 1978; Dohrmann *et al.*, 2013a), but to do this they need to maintain their favourable properties such as their swelling and sorption capacity against heat impacts in an engineered barrier system (EBS), predominantly to ensure that diffusion is the dominant transport mechanism (Sellin & Leupin, 2013). In some countries, the maximum thermal load that bentonite may be exposed to is already predetermined in disposal concepts. In other countries, this parameter is still under discussion. Accepting higher temperatures of the canister at the metal/bentonite interface would enable the disposal of higher volumes in the canister while the space demands of the entire repository would be reduced.

Examples of high-temperature concepts in clay host rock include ventilation systems that allow a maximum backfill inner-

surface temperature of close to 300°C (Greenberg *et al.*, 2013), with the backfill composed of bentonite and sand. Increased temperatures will impact both the bentonites used in the EBS as well as the host rock. In such a setting, bentonites in EBSs would be closer to the canisters and accordingly subjected to higher temperatures than the host rock. EBS materials would, in this scenario, see reductions in some of their favourable properties such as sorption and swelling, and they act as a kind of sacrificial material in the hottest parts. In the cooler parts, EBS materials would maintain their original characteristics. Thus, EBS design has to take the expected temperatures into account while also considering the nature of the host rock.

In the Finnish and Swedish KBS-3 concept for crystalline rock, the maximum temperature allowed was set to <100°C to avoid loss of swelling capacity of smectites (Sellin & Leupin, 2013). The concept was tested in a full-scale prototype repository *in situ* in Äspö, Sweden (Johannesson *et al.*, 2007). Under these comparatively low temperatures, Dohrmann & Kaufhold (2014) barely detected any clay mineralogical changes at distances >1 cm from contact with the heater. Only the cation-exchange capacity (CEC) decreased slightly more in bentonite blocks that

Corresponding author: Stephan Kaufhold; Email: s.kaufhold@bgr.de

Cite this article: Kaufhold S, Dohrmann R, Wallis I, Weber C (2023). Chemical and mineralogical reactions of bentonites in geotechnical barriers at elevated temperatures: review of experimental evidence and modelling progress. *Clay Minerals* 58, 280–300. <https://doi.org/10.1180/clm.2023.26>

© The Author(s), 2023. Published by Cambridge University Press on behalf of The Mineralogical Society of the United Kingdom and Ireland. This is an Open Access article, distributed under the terms of the Creative Commons Attribution licence (<http://creativecommons.org/licenses/by/4.0/>), which permits unrestricted re-use, distribution and reproduction, provided the original article is properly cited.

were subjected to higher temperatures compared to other blocks; however, the changes were only marginally outside of analytical error. In clay-based repositories, where the host rock is considered to be the main barrier, higher temperatures in contact with bentonite buffer materials can be applied (Sellin & Leupin, 2013). However, temperatures >100°C may lead to boiling in cases of pressure relief in the system (e.g. Greenberg *et al.*, 2013). This could occur through cracks in the host rock and is more probable in the case of crystalline rocks compared to clay host rocks. Boiling was observed in the upper part of the second alternative buffer material test (ABM-2; Table 1; Dohrmann & Kaufhold, 2017) while investigating the integrity of compacted bentonites as well as pellets and marine clays assembled in cages. These latter parts of the barrier were possibly not tight enough to prevent pressure loss. The pressure loss led to boiling, which in turn caused significant precipitation of halite and disintegration of some of the blocks. As a result, 100°C can be considered a reasonable temperature limit during the early phase of installation because the pressure is not high enough to raise the boiling point of water. With additional sealing or encapsulation in a tight host rock, the temperature, however, could also be higher.

In sum, research to date suggests that it appears reasonable to fix the maximum canister temperature to <100°C in cases of crystalline host rocks. In cases of other host rock materials, in which pressure relief caused by cracks is less likely to occur, other geochemical reactions that take place at a specific canister temperature could provide the basis for the maximum allowable temperature. As an example, the dehydroxylation temperature of smectite, which starts at ~300°C (Kuligiewicz & Derkowski, 2017), would be the ultimate temperature at which smectites degrade. Goethite, which can be present as a bentonite admixture, would dehydroxylate at 300°C. At lower temperatures, dehydration of smectite interlayers is observed, starting at <100°C ranging up to 200°C. These reactions, however, were only observed in open systems, in which water was able to leave the clay surface. In an intact EBS, water transport is limited, and one would rather observe equilibration at a temperature-dependent humidity level (e.g. Fernandez *et al.*, 2018). This will strongly depend on the initial water content of the bentonite, as shown experimentally for bentonite–halite mixtures at elevated temperatures (Kaufhold *et al.*, 2009). Moreover, dehydration does not cause the structural breakdown of smectite (as dehydroxylation does), but it is known to cause some loss of swelling capacity, presumably due to cation fixation in the interlayer of smectite (Endell, 1939; Kaufhold & Dohrmann, 2010a). The degree to which this effect might be reversible is not yet known. The most important reactions with respect to the EBS in water-saturated systems might be dissolution/precipitation processes. These reactions often follow the Arrhenius law, and in the case of most minerals present in bentonites, solubility increases with increasing temperature, thus accelerating the alteration process. Lowering the temperature will decrease the reaction rate, but the principal reactions would still occur. Therefore, dissolution/precipitation processes alone are not suitable to set a maximum canister temperature. To derive a safe maximum canister temperature, all relevant physico-chemical processes that could impact the integrity of the barrier at a given temperature have to be considered simultaneously. Currently, this can only be achieved through numerical modelling, which has been shown to provide a useful framework to integrate, quantify and, ultimately, better understand the thermally induced, coupled chemical and mineralogical reactions and their impacts on solute migration within barrier systems.

Modelling of EBS designs, however, comes with unique challenges, as it relies on accurate thermodynamic datasets that have to cover a larger range of clay mineralogy.

Thermally induced chemical and mineralogical reactions in bentonites have been investigated both in the laboratory and after sampling of long-term deposition tests (large or medium scaled; Table 1). In the laboratory, it is possible to control the amount of water and the composition of the water (if present), neither of which is possible in deposition tests. It is, for instance, possible to investigate the integrity of bentonites under dry conditions at the laboratory scale. This led to partial cation fixation and decreases in CEC in experiments reported, for example, by Endell (1939), Hofmann & Klemen (1950) and Kaufhold & Dohrmann (2010a). In these laboratory tests, water was largely absent. In an actual repository, it will be difficult to reach such dry conditions both because of the prevailing humidity and because industrially produced bentonites will be used, which will contain at least a few mass% of water.

Similarly, illitization can be investigated in the laboratory, which is barely observed in larger-scale deposition tests. Processes that are restricted to interfaces can also be investigated appropriately at the laboratory scale, as the relevant components can be mixed as powders (e.g. cement and bentonite or iron and bentonite), which then enables bulk sample analysis. However, large- or medium-scale deposition tests allow thermal gradients to evolve, which trigger hydrogeochemical reactions with gradients not observable in laboratory experiments (e.g. Mota-Heredia *et al.*, 2023). In addition, the impacts of low water/rock ratios, which are typical of an actual repository, are rarely reported in laboratory studies and generally require the use of natural analogues. Both types of experiments have their specific value and should both be considered when discussing thermally induced reactions in bentonites.

In the present study, data and results are discussed that were derived from the authors' analysis of large-scale tests and their respective materials. An overview of the tests that were analysed and reported before and are discussed again in the present study is provided in Table 1. Thereby, the dimensions of real-scale tests depend on the concept employed, but the diameter of the heater is typically in the range of 1 m. The ABM medium-scale tests consisted of a 10 cm-diameter heater surrounded by 30 cm compacted bentonite rings.

The most significant hydrothermally induced reactions of bentonites identified through laboratory and heated large-scale deposition tests are:

- Cation exchange
- Decrease or increase of CEC (affecting swelling and hydraulic properties)
- Dissolution/precipitation (redistribution) of (partly) soluble phases as carbonates and sulfates and sometimes even of silicates such as cristobalite or zeolite
- Oxidation of pyrite
- Mg enrichment at the heater
- Formation of corrosion products at the heater contact (Fe-silicate or Fe-carbonate, depending on carbonate and Si abundance)
- Dissolution of smectite and precipitation of secondary silicates both at the iron (carbon steel)/bentonite and cement/bentonite interface

The present paper aims to summarize thermally induced and thermally affected reactions in bentonites, as identified in

Table 1. Overview of real- and medium-scale tests investigated and discussed in the present study.

	TBT temperature buffer test	PTR prototype repository test – section 2	LOT-A2 long-term test	ABM-1 alternative buffer material test	ABM-2 alternative buffer material test	ABM-5 alternative buffer material test	FEBEX full-scale engineered barrier experiment
Mineralogical publication(s)	Svensson & Hansen (2013)	Olsson <i>et al.</i> (2013), Dohrmann & Kaufhold (2014)	Karland <i>et al.</i> (2009)	Dohrmann <i>et al.</i> (2013b), Kaufhold <i>et al.</i> (2013), Svensson & Hansen (2013), Svensson (2015)	Kumpulainen <i>et al.</i> (2016), Dohrmann & Kaufhold (2017), Kaufhold <i>et al.</i> (2017)	Kaufhold <i>et al.</i> (2021)	Fernández <i>et al.</i> (2018), Kaufhold <i>et al.</i> (2018)
Implementor	SKB	SKB	SKB	SKB	SKB	SKB	NAGRA
HRL/URL	Äspö	Äspö	Äspö	Äspö	Äspö	Äspö	Grimsel
Buffer	MX80 bentonite	MX80 bentonite	MX80 bentonite	11 different clays in 30 blocks	11 different clays in 31 blocks	11 different clays in 30 blocks	Almeria bentonite (FEBEX)
Heater	Carbon steel	Copper	Copper	Carbon steel	Carbon steel	Carbon steel	Carbon steel
Scale	Real-scale	Real-scale	Medium-scale	Medium-scale	Medium-scale	Medium-scale	Real-scale
Heating phase	7 years	8 years	6 years	28 months	6.5 years	4 years	18 years
Maximum temperature	150°C	85°C	5.5 years at 140°C	1 year at 130°C	3–4 years at 141°C	6 months at 250°C	100°C

HRL = hard rock laboratory; URL = underground rock laboratory.

laboratory experiments, medium- to large-scale deposition tests and natural analogue studies, and to discuss current challenges in integrating these into numerical modelling frameworks. Physicochemical properties such as swelling and hydraulic conductivity (amongst others) are also affected by temperature (e.g. Kale & Ravi, 2018), but these are not the subject of the present review.

Cation exchange

All large-scale deposition tests in crystalline rock that reached full water saturation showed significant cation exchange caused by uptake of ambient groundwater from the host rock. Following glaciation cycles, groundwater chemistry in crystalline rocks at repository depth will change over time, with the lowest electrolyte concentration occurring after melting of the ice shield. A bentonite buffer in a repository will interact with the groundwater in such a way that the cation exchange population will constantly re-equilibrate with the cations in the groundwater. Interaction of groundwater with a relatively high salinity – as, for example, at Äspö, Sweden (Na–Ca–Cl type; e.g. Muurinen, 2006) – with bentonite may differ from interaction at other test sites exhibiting lower salinities, which can result from post-glacial phases. A lower salinity of the host rock water can be found in the Grimsel test site (GTS) in Switzerland (Na–Ca–HCO₃–F type; Degueldre, 1994). In both cases, cation exchange plays a significant role regarding mineralogical and porewater characteristics in bentonite barriers. Cation exchange occurred within the Svensk Kärnbränslehantering AB (SKB) tests with maximum canister surface temperatures of ~140°C (e.g. Karland *et al.*, 2009; Dohrmann *et al.*, 2013b; Svensson & Hansen, 2013; Kumpulainen *et al.*, 2016), and even at <100°C (Dohrmann & Kaufhold, 2014), as well as in full-scale experiments at the GTS with a relatively low-salinity groundwater at <100°C (Fernandez *et al.*, 2018; Kaufhold *et al.*, 2018). Particularly interesting is the ABM test series, which used different clays with different initial cation populations. Following saturation, the cation population equilibrated with the inflowing groundwater within 1 year. As a consequence, Na-rich bentonites lost most of the exchangeable Na⁺ and increased in exchangeable Ca²⁺, whereas Ca²⁺-rich

bentonites lost parts of the exchangeable Ca²⁺ and took up some exchangeable Na⁺ (Dohrmann *et al.*, 2013b; Dohrmann & Kaufhold, 2017). Interestingly, blocks of the same bentonite material located at different positions within the deposition test exhibited different cation populations. This was explained partly by varying initial conditions (i.e. water saturation during heating or before heating commenced) as well as subtle differences in the temperature that each bentonite block was exposed to depending on its location in relation to the heaters. In addition, cation population differences were correlated with the adjacent host rock characteristics. Rock fractures and rock permeability to groundwater adjacent to bentonite blocks governed water inflow. Chloride in the porewaters of different blocks equilibrated between the neighbouring blocks, starting from very different initial chloride concentrations in the different reference materials.

In summary, one can state that the cation exchange in the ABM tests was a rapid process. Considering the performance of a particular bentonite, the chemical composition of the porewater appears to be more relevant than the initial cation population of the smectites.

Cation-exchange reactions are commonly included in geochemical reaction models, and their computation according to the Gaines–Thomas, Gapon, Vanselow and Rothmund–Kornfeld conventions, allowing for both equilibrium and kinetically controlled exchange reactions, is routine (e.g. Parkhurst & Appelo, 1999, 2013). In barrier systems, the exchange reactions are limited by solute transport rates (e.g. the diffusion rate of solutes into the barrier). Modelling of ion-exchange reactions in diverse clays and bentonites has been reported – for example, onto MX80 bentonites (e.g. Chaparro *et al.*, 2021), Na-, K- and Ca-smectites (Missana *et al.*, 2014), biotite (Kyllönen *et al.*, 2014) and pure illites (e.g. Liu *et al.*, 2004; Cherif *et al.*, 2017), as well as natural argillaceous rocks such as Boom Clay or Opalinus Clay (e.g. Bradbury & Baeyens, 2000) and synthetic Na-saturated smectites (Ferrage *et al.*, 2011) for a range of radionuclides and other solutes.

Single-exchanger site models (Wallis *et al.*, 2016; Chaparro *et al.*, 2021) as well as multi-site numerical representations of clay minerals have been employed (Liu *et al.* 2004; Tournassat *et al.*, 2007; Fuller *et al.* 2014). Multi-site ion-exchange models

thereby simulate different types of ion-exchange sites on clays, including basal planes on crystal surfaces and interlayer sites on crystal edges. Notably, the number of interlayer sites (~80–90% of the CEC depending on pH; Vogt & Köster, 1978; Kaufhold & Dohrmann, 2013; Christidis *et al.*, 2023) exceeds the number of edge sites. All models require representative exchange constants for the respective ion-exchange reactions. While some authors have employed fixed exchange constants in accordance with readily available thermodynamic databases (Chaparro *et al.*, 2021), many studies determined selectivity coefficients based on retention experiments of solutes onto clay minerals under specific pH values, ionic strengths and radionuclide concentrations. This guarantees a consistent set of coefficients for the simulation under the specific laboratory or field study conditions (e.g. Kyllönen *et al.*, 2014; Missana *et al.*, 2014; Baborová *et al.*, 2018).

A survey of experimental data regarding cation-exchange isotherms for clays and related materials, which includes temperature-dependent data, is presented in Bruggenwert & Kamphorst (1981). Apart from material-specific data and chemical information about the liquid phase, these authors present selectivity coefficients and, if available, free energies, enthalpies and entropies of the exchange reactions. In addition to the references presented in Bruggenwert & Kamphorst (1981), relevant materials, including kaolinite, bentonite, soils and vermiculite, have been studied by Assad *et al.* (1981), Doula *et al.* (1995), Udo (1978), Inoue (1984) and Itälä & Muurinen (2012). Note that this short list of references is certainly not exhaustive, but, together with the aforementioned tabulation, it provides an overview of the available data. These studies demonstrate that selectivity coefficients depend on the exchanger composition, the ambient temperature and the solution chemistry. The intricate interplay of these factors hinders a systematic discussion of the data at hand because a variety of materials have been studied in various solution chemistries and at different temperature intervals. The interested reader can consult Bruggenwert & Kamphorst (1981) as well as Maes & Cremers (1981) for more information.

Considering the thermodynamic data (exchange constants, free energy, enthalpy and entropy of exchange), some qualitative features that are present in the majority of data in Bruggenwert & Kamphorst (1981) can be highlighted. Considering the homo-valent exchange of monovalent ions, it is noted that the enthalpic and entropic contributions to the free energy of exchange both appear to be negative, with the resulting free energy then negative as well. In systems where the initially adsorbed cation is monovalent and the one to be adsorbed is divalent, the situation becomes somewhat more complicated. For initially adsorbed sodium and a divalent exchanger ion, the enthalpy and entropy become positive quantities; however, the free energy remains negative. The total free energy of exchange appears to be entropically dominated in these systems, indicating that one can expect a notable modification of the exchange equilibrium with sufficiently large temperature intervals. If the initially adsorbed cation is either ammonium, potassium or caesium and the exchange ion is divalent, enthalpy and entropy remain positive, but now the free energy of exchange can become positive. These qualitative features apply to the majority of specified systems in cases of alkali, earth alkali and NH_4^+ ions. For systems involving trivalent ions, the authors were not able to find values for the enthalpy and entropy of exchange.

From this rather short and incomplete discussion of temperature-dependent cation exchange, it is evident that even

establishing a consistent database of exchange constants is rather difficult. Systematic studies on well-defined materials under relevant conditions (solution chemistry and temperature) will be necessary to establish consistent exchange constants and associated thermodynamic parameters. In view of the complex mineralogical composition of barriers and host rocks (both of which probably have mixed initial cation populations) and the complex nature of groundwater, critical testing of such a database is mandatory.

Cation fixation

Clay scientists were aware of the fact that the CEC of bentonites can be reduced by thermal treatment before large-scale deposition tests were available. Long-term laboratory tests (Kaufhold & Dohrmann, 2010a) showed that exchangeable cations can be fixed by the smectite structure, which means that these cations neither are exchangeable nor hydratable anymore (e.g. Mackenzie, 1963; Inoue, 1983). After heating at 90°C for 1.5 years, ~9% of the cations of 38 bentonites were fixed, which means that they were not exchangeable any more using the standard CEC routine (2 h shaking with Cu-trien). After 4.5 years at 120°C, 14% of the cations were fixed (non-exchangeable). Hence, only 5% more cations were fixed despite increasing the temperature by 30°C and despite a threefold increase in time (Kaufhold & Dohrmann, 2010a). These numbers indicate that the process of cation fixation may be limited. In addition, the prerequisite for cation fixation is a dry environment, which is unlikely to be representative of an actual repository because of the humidity in the repository and the fact that industrially produced bentonites contain at least a few mass% of water. However, in some concepts, the bentonite will be installed with lower water contents (Sellin & Leupin, 2013). The advantage of using dry bentonite is that higher dry densities can be produced with the same compaction load. In such systems, cation fixation may be important at the beginning when it is comparably dry. Under wet conditions, which will prevail later on, cation fixation will be less important.

Cation fixation can be determined by cation-exchange experiments in which ideally both the CEC and the exchangeable cations are measured. According to Gu *et al.* (2001), who used transmission electron microscopy (TEM) to detect amorphization in the high-vacuum environment required for TEM, a decrease of the CEC was observed only at >400°C, which indicates that precise CEC measurements are required in order to determine cation fixation much below 400°C.

The mechanism(s) leading to this cation fixation are not well understood to date, and they probably differ depending on the type of cation and possibly the crystal chemistry or the layer charge density of smectites. Because of its low hydration energy, K^+ is believed to enter the ditrigonal cavities where it can be fixed (Horvath & Novak, 1976). Small cations such as Li^+ and Mg^{2+} could theoretically migrate into the dioctahedral vacancies of the octahedral sheet, but this is still under discussion (Kaufhold *et al.*, 2016). Ca^{2+} and Na^+ are also fixed by thermal treatment (e.g. Kaufhold & Dohrmann, 2010a), although they are apparently too large to migrate into the octahedral vacancies. They hence are supposed to remain within the ditrigonal cavities of the tetrahedral sheet, similarly to fixed K^+ . Eberl & Hower (1977) observed Na^+ fixation along with formation of paragonite, indicating dissolution and precipitation. Hofman & Klemen (1950) also observed decreasing amounts of exchangeable Ca^{2+}

and Na⁺ upon heating, but the temperatures were much larger than those relevant for a repository of most concepts (>300°C). According to Weiss & Koch (1961), cation fixation depends on cation size and octahedral vacancies. Notably, cation fixation was observed if the samples were heated under dry conditions. In addition, Mg²⁺ could only be fixed under dry conditions (Kaufhold *et al.*, 2016). One of the remaining open questions is whether fixed cations can be rehydrated using higher temperatures and excess water, which remains to be investigated in future experiments.

At the contact with the heater of large-scale deposition tests, both decreases and increases of the CEC have been observed (Dohrmann & Kaufhold, 2017), which is particularly interesting regarding the ABM tests where different bentonites, which were exposed to similar conditions, exhibited different reactions (Fig. 1). The CEC decrease could be explained by cation fixation. The CEC increase, however, is more difficult to explain.

A CEC decrease can be explained either by cation fixation, by smectite alteration (dissolution and precipitation as a non-swelling phase), by pH change caused by cation exchange or through pyrite oxidation and/or by dilution caused by the precipitation of other phases (addition of Fe minerals as an example

would lead to a decrease in the smectite content). An increase in the CEC would indicate an increase in the smectite content, which is not likely to occur but cannot be excluded. The increase, however, could be explained by 'reactivation' or 'liberation' of previously fixed cations caused by water and elevated temperature or by an increased pH value caused by exchange of Ca²⁺ for Na⁺ (interlayer Na⁺ leads to higher pH values in equilibrium with a solution; Kaufhold *et al.*, 2008).

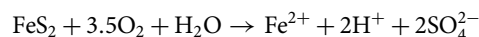
One could assume that the same bentonites would show the same trend in the ABM tests (either decrease or increase in the CEC). However, this was only partially what was observed. The MX80 blocks both at the top and the bottom of the experiment all showed a marked decrease in CEC, accounting for ~10% of the initial value. However, in block 14, which was installed in the central part and manufactured from MX80 granulates, an increase in the CEC was observed (Fig. 1). Other bentonites also showed marked differences between blocks of the same material installed at different locations within the ABM tests. This indicates that locally varying conditions were more important with respect to the decrease or increase in CEC than the type of bentonite.

The presence of water in combination with heat, leading to partial smectite dissolution, could possibly explain why the CEC of the bentonite at the contact with the heater in large-scale tests sometimes increases and sometimes decreases. Accordingly, the most important parameter determining either CEC increase or CEC decrease would be water content, followed by the amount of initially fixed cations (the CEC could not increase because of rehydration of fixed cations if the smectite did not contain any fixed cations in the reference material). The amount of fixed cations is suspected to be related to the layer charge density in such a way that high-charge smectites contain more fixed cations than low-charge ones (Kaufhold *et al.*, 2011).

In summary, a portion of all common interlayer cations can be fixed under dry conditions at elevated temperatures, rendering them non-exchangeable. The fixed cations either reach an octahedral vacancy (if they are small enough) or reside within the ditrigonal holes. As the process of cation fixation and possible cation re-liberation is still under discussion, there are insufficient data to include this phenomenon in numerical modelling codes.

Oxidation of pyrite

Claystones as well as some bentonites were formed under anaerobic conditions. Under these conditions, pyrite forms upon (beginning) diagenesis from iron mono-sulfide precursors (e.g. Hunger & Benning, 2007). As soon as a claystone or bentonite is excavated, pyrite becomes unstable and might oxidize, often forming either jarosite or gypsum (Uzarowicz & Skiba, 2011). Pyrite is considered to be particularly important for the EBS because it can cause Cu corrosion, act as microbial feed, decrease the pH and buffer the Eh. The initial pyrite alteration reaction is the oxidation of Fe-disulfide to sulfate by oxygen:



At acidic pH, ferric iron may trigger pyrite oxidation, but such low pH values are hardly expected to occur in the barrier systems because the smectites of the bentonites buffer the pH (e.g. Kaufhold *et al.*, 2008). Depending on the chemical environment,

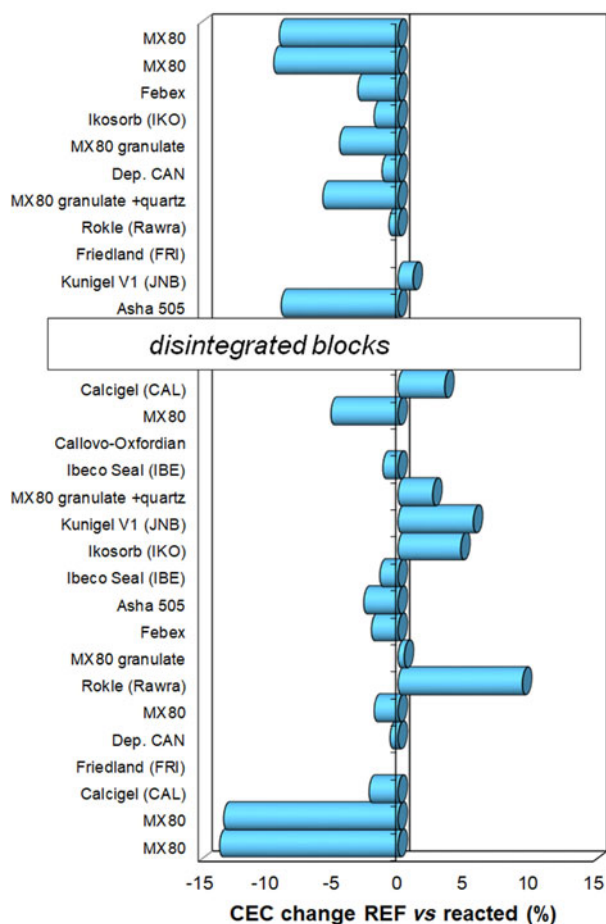


Figure 1. Bar graphs indicating percentage CEC differences of the reacted samples at the end of the test for the 2–8 cm samples (averages) for all bentonite blocks in comparison to the reference materials (REF) of the ABM-2 test (Dohrmann & Kaufhold, 2017). Note that negative values indicate a CEC decrease. From Dohrmann & Kaufhold (2017). Reproduced with kind permission of The Clay Minerals Society, publisher of *Clays and Clay Minerals*.

Fe²⁺ remains in solution, oxidizes to Fe-oxohydroxides (Bingham & Nordström, 2000) or forms Fe-sulfate. The protons could lead to hydrolysis of aluminosilicates, hence promoting their weathering, and this may lead to dissolution of carbonates (Pye & Miller, 1990), which in turn would affect porosity (Mazurek *et al.*, 2011). Sulfate may precipitate as gypsum or jarosite.

At a molecular level, insight into this reaction was gained from density functional theory modelling, which showed the different activation energies of the various steps of the oxidation (Dos Santos *et al.*, 2016). The mechanism was recently further discussed by Feng *et al.* (2019), who stated that the mechanism of pyrite oxidation is still not well understood.

The oxidation of pyrite is not necessarily induced by elevated temperature but by moisture and oxygen, and hence it is not exclusively a thermally induced reaction. However, with regard to assessing the stability of bentonite (clay) barriers, this reaction has to be considered and included in geochemical modelling. In the ABM-5 test, which operated at 250°C (maximum), Kaufhold *et al.* (2021b) demonstrated that pyrite was oxidized in some samples but was preserved in others. Notably, the pyrite already found in the reference materials survived excavation in the mine and industrial production, as it was still present in the industrially dried and milled reference material. After the ABM test, pyrite was sometimes still present and oxidized elsewhere. In the ABM-2 test ($T_{\max} = 140^{\circ}\text{C}$), pyrite, if it was initially present in the materials (MX80, JNB, FRI and IBE), was absent (Kaufhold *et al.*, 2017). However, the ABM-2 test was characterized by high water ingress from the ambient rock, with precipitation of anhydrite observed in many blocks, possibly caused by boiling due to a pressure drop towards the surrounding crystalline rock (Dohrmann & Kaufhold, 2017).

Pyrite stability and the resulting geochemical environments have been studied extensively, particularly in the field of acid mine drainage, for almost 40 years (e.g. Psenner, 1983; Moses *et al.*, 1987; Nordstrom, 2011). Modelling the stability of pyrite relies on kinetic rate expressions. Rate laws for pyrite oxidation in air have been developed and are used in, for example, mine waste dam models for acid prediction (e.g. Jerz & Rimstidt, 2004). Aqueous pyrite oxidation rate laws, which are applicable for saturated media, have been studied extensively by Williamson & Rimstidt (1994), Holmes & Crundwell (2000) and Rimstidt & Vaughan (2003) and have led to the widely accepted rate of aqueous pyrite oxidation by O₂ (Equation 1):

$$r_{\text{pyr}} = k_{\text{pyr}} C_{\text{O}_2}^{0.5} C_{\text{H}^+}^{-0.11} \quad (1)$$

where r_{pyr} is the pyrite oxidation rate (mol m⁻² s⁻¹), k_{pyr} is the rate constant (mol m⁻² s⁻¹) at 25°C, C_{O_2} is the concentration of dissolved oxygen (mol L⁻¹) and C_{H^+} is the concentration of protons (mol L⁻¹).

The rate expression reveals a strong dependency on the oxygen concentration, while the effect of pH on the rate is small. The above is applicable for environments in the pH range of 3–10 and has been used in numerous geochemical modelling studies covering field and laboratory investigations. For instance, Appelo *et al.* (1998) successfully simulated the oxidation of pyrite in marine sediments. Other authors have quantified the release of trace metals following pyrite oxidation (e.g. Fakhreddine *et al.*, 2016; Wallis & Pichler, 2018). Eckart & Appelo (2002) extended the rate expression to include pyrite oxidation by nitrate, while Prommer & Stuyfzand (2005) included a temperature dependency

using the Arrhenius equation to evaluate geochemical changes in response to temperature variation in a deep-well injection experiment into a pyritic aquifer.

Geochemical modelling as well as experimental studies show, however, that due to the diversity of physical and chemical properties in environmental systems, the pyrite oxidation rate expression has to be tailored towards specific environments. It is often observed that different sediments behave quite differently with respect to the extent of pyrite oxidation after excavation of a sample. After excavating a sample of the marine Friedland Clay (north Germany), it takes only hours until up to a few millimetres-long gypsum needles can be observed macroscopically. The same observations can be made with Opalinus Clay, showing the formation of cracks along with the growth of gypsum. Other clays can be stored for years in the laboratory atmosphere without any significant pyrite oxidation. One probable reason for the different tendencies of pyrite to oxidize is the trace elemental composition. According to Gregory *et al.* (2017), pyrites with a higher content of trace elements oxidize faster, but Co and Ni can stabilize the lattice. This effect can hardly be accounted for in modelling in which, however, the exposed surface area should be considered. For instance, framboidal pyrite, which consists of submicron-sized crystals (Fig. 2a) and therefore has a large surface area, oxidizes at faster rates than, for example, larger-sized pyrite grains (Fig. 2b; Rimstidt & Vaughan, 2003). The properties of the pyrite surface may also change and lead to a slowing of the oxidation reaction with time. An example is the reduction in oxygen diffusion into pyrite crystals through the increasing size of the oxidized shell, which progressively surrounds the unoxidized mineral core as pyrite oxidation progresses (e.g. Elberling *et al.*, 1994). Others have reported saturation of the pyrite mineral surface by precipitates of Fe(OH)₃ and iron sulfates as oxidation progresses (Jerz & Rimstidt, 2004; Verron *et al.*, 2019). To account for changes in surface area or reactivity due to, for example, mineral ageing as pyrite dissolves, rate expressions frequently include a dependency of the pyrite oxidation rate on the surface area of the mineral (e.g. Appelo *et al.*, 1998) or employ an oxygen diffusion-controlled shrinking core model that describes the decrease in oxidation rate through an accumulating oxidation shell surrounding pyrite grains that acts as a diffusion barrier for O₂ transport as time progresses (e.g. Davis & Ritchie, 1986; Elberling *et al.*, 1994).

In natural environments, the rate of pyrite oxidation is accelerated by microbial processes (Kappler *et al.*, 2021). Therefore, some authors have introduced a microbial acceleration factor into the rate expression to simulate the impact of biological activity on pyrite oxidation rates (e.g. Kohfahl & Pekdeger, 2006). Microbial processes are known to accelerate the oxidation process by several orders of magnitude under acidic pH conditions (e.g. Nordstrom & Southam, 1997). However, even at circumneutral pH, rates of microbial pyrite oxidation can be an order of magnitude higher than abiotic rates.

Correlated to microbial activity, temperature also affects the rate of pyrite oxidation (Lefebvre *et al.*, 2001). For moderate temperatures, the temperature dependence of pyrite oxidation is adequately described by the Arrhenius equation (Prommer & Stuyfzand, 2005). However, high-temperature environments may limit reaction progress due to a reduction in microbial activity as a result of cell death under higher temperatures. As a result, microbially mediated reaction rates, such as those observed for pyrite oxidation, decline at temperatures that exceed the optimum temperature for microbial activity (Lefebvre *et al.*, 2001; Xie *et al.*,

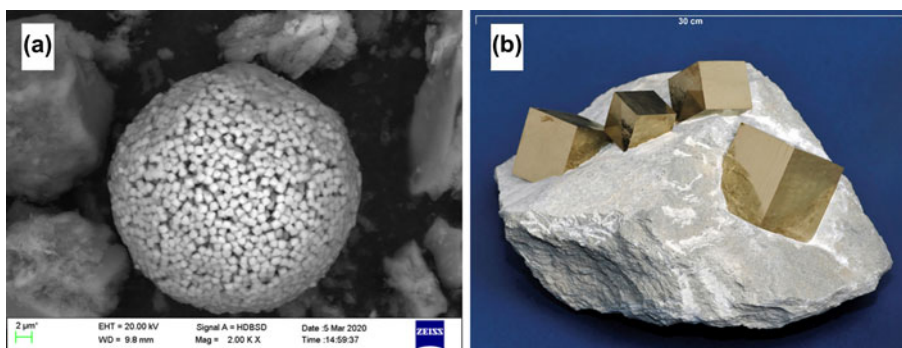


Figure 2. (a) Framboidal pyrite and (b) macroscopically perfect crystals that grew in a clay from Navajún (Spain).

2007). As a consequence, some authors have included an inhibition factor in the pyrite oxidation rate expression for elevated temperatures (e.g. Yi *et al.*, 2021). In this context, it should be noted, that increased temperatures can be naturally achieved in reactive pyritic rock due to the exothermic nature of pyrite oxidation processes (Lefebvre *et al.*, 2001; Amos *et al.*, 2015).

Pyrite is supposed to be the main sulfide phase in both clays-tones and bentonites, but theoretically mono-sulfides such as mackinawite (FeS) and greigite (Fe₃S₄) could also exist (Hunger & Benning, 2007) or form at interfaces such as between bentonite and the canister. Different mono-sulfides were found after excavating bentonite from the Full-Scale Engineered Barrier Experiment (FEBEX; Fernandez *et al.*, 2018).

In summary, pyrite stability depends on the exposed surface area of pyrite, which in turn depends on particle size and crystallinity and trace elemental composition, but also on temperature, oxygen concentration, internal porewater chemistry (e.g. pH, availability of ferric iron), microbiology and water content. For reasonable inclusion of pyrite oxidation into geochemical models, empirical studies on the pyrite characteristics within the employed bentonite should be conducted and existing oxidation rate expressions adjusted accordingly.

Dissolution and precipitation

Carbonates, gypsum and anhydrite

The long-term test conducted by SKB in Äspö (LOT; Table 1) was the first *in situ* experiment in which a redistribution of sulfate in the compacted bentonite was observed (Muurinen, in Karnland *et al.*, 2009). At the start of the experiment, gypsum was evenly distributed, with a sulfate content of 0.27 mass% throughout the blocks (dashed blue line in Fig. 3). After the test, the retrieved blocks were analysed at different distances from the heater. Samples collected near the crystalline rock showed a slightly lower sulfate content, but a maximum concentration was observed approximately in the centre of the blocks at a distance of ~4 cm. The contact sample at the Cu heater showed slightly increased sulfate values compared with the 1 cm sample, which could be explained by the formation of the corrosion product Cu(Fe)S. This redistribution of sulfate was modelled successfully based on the observed thermal and hydraulic gradients by Arcos *et al.* (2000). The authors simulated the behaviour of the bentonite accessory minerals calcite, anhydrite, siderite, pyrite and quartz during the thermal stage and highlighted the relevance of the cation-exchange population of the bentonite. The authors also demonstrated that cation-exchange reactions controlled the concentration of calcium, which, in turn, controlled the precipitation

and dissolution of calcite. With calcium being the dominant ion within the bentonite porewaters, anhydrite ‘migrated’ towards the clay/crystalline rock interface *via* dissolution and precipitation. They concluded that cation-exchange processes probably dominate the ionic inventory within the bentonite, even after 100,000 years.

In the LOT experiment (Fig. 3), only MX80 bentonite was used. In the ABM tests, in which different bentonites with different S contents and different hydraulic properties were used, different S redistribution patterns were identified. In the first alternative buffer material test (ABM-1), S enrichment at the contact with the heater was observed for some bentonite blocks, which resulted from the precipitation of anhydrite (e.g. sample FEB, ABM-1; Kaufhold *et al.*, 2013). Other blocks, however, showed slightly decreasing S concentrations towards the host rock, and others showed unchanged concentrations. In the ABM-2 test, unchanged gypsum concentrations were found in the top and the bottom bentonite blocks, and significant anhydrite precipitation was observed where boiling occurred as a result of a local pressure relief (Dohrmann & Kaufhold, 2017). It is assumed that the water vapour left the system *via* a leakage in the barrier and presumably the crystalline rock as well. Gypsum, in conclusion, is a rather soluble component of some bentonites and readily dissolves and precipitates within the barrier. The thermodynamic constants of gypsum are well known (e.g. Nordstrom, 2013; Shen *et al.*, 2019). Accordingly, the fate of gypsum in different barrier systems can be simulated on the basis of the time-dependent thermohydraulic conditions within the barrier. The results of the ABM tests are particularly valuable for the verification of gypsum dissolution and precipitation reactions and their modelling because rather different profiles were obtained for different bentonite blocks, which can be used to verify model results. According to Karnland (1995), gypsum redistribution is favoured by a high buffer density, a low content of accessory minerals, a low electrolyte content in the surrounding water and a high water pressure.

Carbonates are less soluble than gypsum, but results obtained from different large-scale tests showed that carbonates can also dissolve and precipitate throughout the barrier system, similarly to gypsum. In the ABM-1 test, inorganic carbon enrichment was detected only at the contact with the Fe heater. This could, therefore, be related to the corrosion process in which sometimes siderite forms. The C needed for siderite formation may be derived from initially present carbonates in the bentonite, from C contained in the carbon steel or from CO₂/HCO₃⁻ present in the (inflowing) porewater. In the ABM-2 test, in which boiling occurred in the upper part of the core, a decrease in the carbonate content was detected. In the lower part, however, calcite showed

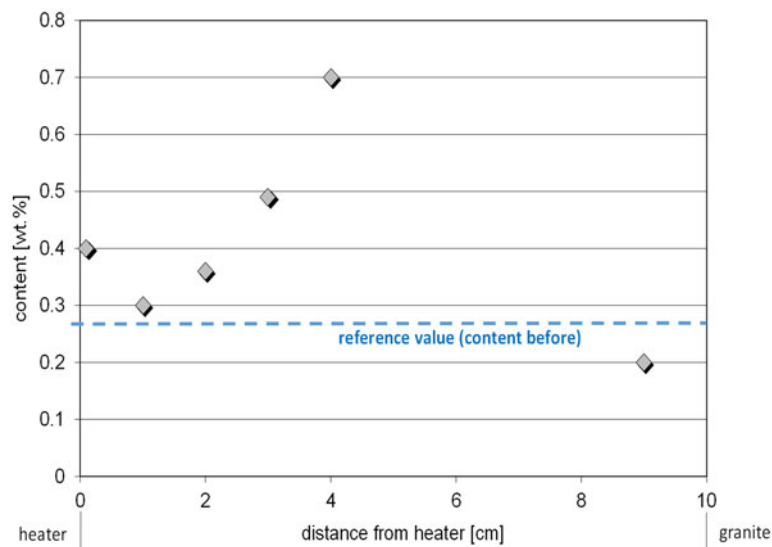


Figure 3. Sulfur (determined by LECO C-S analyser; Karnland *et al.*, 2009) redistribution in the LOT A2 experiment (Table 1). The dashed blue line represents the initial sulfur content resulting from both pyrite and gypsum.

only minor variation. A special reaction was observed in ABM-5 (Kaufhold *et al.*, 2021). Because of the absence of the paraffin-rich lubricant Molykote® (DuPont), which in the other tests was used to support canister emplacement, the CO₂ signal derived from simultaneous thermal analysis could be unambiguously related to siderite, which formed as the calcite concentration decreased (Fig. 4). This process probably occurred in the other ABM tests as well but could not be detected unambiguously because of the presence of Molykote BR-2 Plus. The formation of siderite was restricted to the iron/bentonite interface. Several authors identified magnetite and Fe-silicate as the main corrosion products (Lantenois *et al.*, 2005; Wilson *et al.*, 2006a, 2006b; Perronet *et al.*, 2007; Carlsson *et al.*, 2008; Osacky *et al.*, 2010; Kaufhold *et al.*, 2015). In some corrosion studies, carbonates were added. These studies found siderite as a corrosion product either along with Fe-silicates and magnetite or even alone (Savoye *et al.*, 2001; Martin *et al.*, 2008; Romaine *et al.*, 2013; Mendili *et al.*, 2014). Modelling the long-term behaviour of the corrosion interface showed that siderite will be an important phase (Savage *et al.*, 2010) and that the initial Fe-silicates will recrystallize. In archaeological artefacts used as natural analogues (Saheb *et al.*, 2010,

2013), magnetite and siderite were the dominating corrosion products.

The macroscopic dissolution and precipitation kinetics of the bentonite accessory minerals carbonate, gypsum and anhydrite are routinely approximated as an equilibrium reaction because the respective reaction rates are considered ‘sufficiently fast’ compared to the minimal time resolution in the model. Thus, local equilibrium is assumed to be reached instantaneously. For instance, Samper *et al.* (2016) employed a multicomponent reactive transport model to study the long-term interactions of corrosion products and compacted bentonite in a high-level radioactive waste repository in crystalline rock. All mineral reactions, except for canister corrosion, were assumed to be at chemical equilibrium, including calcite and gypsum dissolution and precipitation. Numerical simulations were performed over a time horizon of 1 Ma. Samper *et al.* (2018) simulated the hydrochemical changes within the FEBEX *in situ* test, calibrated on the basis of observed gravimetric water content, dry density, temperature and major ion concentrations. The model spanned a period of 18 years and assumed calcite, anhydrite and gypsum to be at chemical equilibrium over the duration of the experiment. Using this approach,

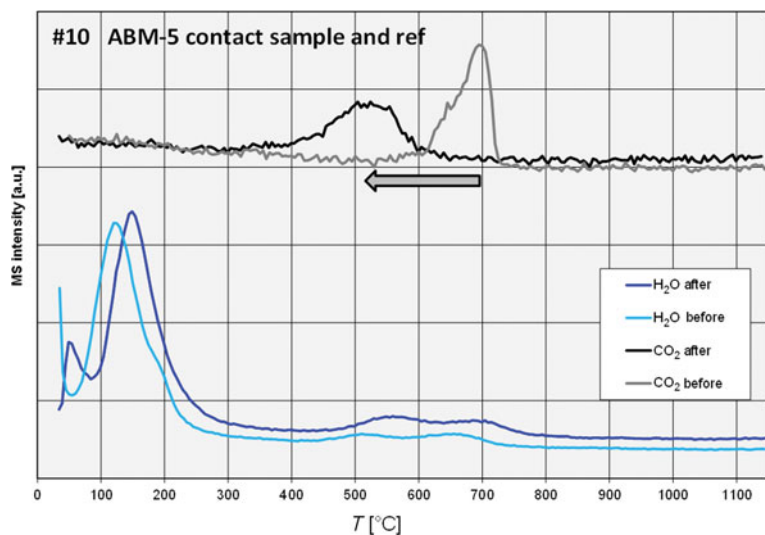


Figure 4. Mass spectrometer (MS) curves of water (blue) and CO₂ (black/grey) of the reference (ref) sample (brighter colour) and contact sample (darker colour) of block 10 from the ABM-5 test (Kaufhold *et al.*, 2021). Before: composition of the ref material used to produce the blocks for the experiment; after: block material retrieved after termination of the experiment. The heating rate was 10 K min⁻¹.

the computed major ion concentrations were broadly consistent with observed porewater concentrations, measured at radial distance from the heater/bentonite interface at the end of a first (year 2002) and second operational phase (year 2015) of the FEBEX experiment. The predicted concentrations of dissolved Ca^{2+} and HCO_3^- were thereby linked to the dissolution/precipitation of calcite and sulfate minerals. The simulated dissolved SO_4^{2-} concentrations underestimated the porewater concentration data, possibly due to uncertainties in the initial amount of gypsum in the bentonite.

A similar approach was followed by Arcos *et al.* (2000), simulating the interaction between bentonite buffer and groundwater over 100,000 years. Calcite, siderite, anhydrite, quartz and pyrite were considered equilibrium reactions, where the solubility constant was scaled on the basis of temperature. Sena *et al.* (2010) simulated the long-term buffer material LOT A2 test at the Äspö Hard Rock Laboratory. The LOT A2 test lasted 6 years and consisted of a heating element encapsulated by a copper tube, which in turn was surrounded by pre-compacted Wyoming MX80 bentonite. Again, the dissolution/precipitation of calcite, anhydrite and gypsum were assumed to be equilibrium reactions, leading one to expect that these mineral phases would demonstrate very fast reactivity under the thermohydraulic and chemical conditions that prevailed during the LOT A2 test. The numerical results predicted the dissolution/precipitation of anhydrite, calcite and silica in the heated bentonite in agreement with data measured at the end of the LOT A2 test. In general, gypsum, anhydrite and carbonate reaction rates do vary with temperature. The solubility behaviour of anhydrite is similar to that of calcite and increases with decreasing temperature at low pressure (e.g. Newton & Manning, 2005). The solubility of gypsum changes only slightly up to temperatures of $\sim 55^\circ\text{C}$ (Reiss *et al.*, 2021).

If the equilibrium approach is considered inadequate, generic kinetic rate laws have been employed, which generally take the reactive surface area and saturation state of the respective mineral into account and can take the form seen in Equation 2:

$$R = r_{\text{mineral}} \left(\frac{A}{V} \right) \left(\frac{m}{m_0} \right)^n f(C) \quad (2)$$

where R is the overall reaction rate ($\text{mol m}^{-3} \text{s}^{-1}$), r_{mineral} is the rate constant ($\text{mol m}^{-3} \text{s}^{-1}$), which is temperature dependent, A is the initial surface area of the mineral (m^2), V is the solution volume (m^3), m_0 is the initial moles of the solid, m is the moles of solid at a given time and n is a coefficient that takes the value of 2/3 for uniformly dissolving/growing spheres and 1/2 for cylinder-shaped grains but is generally determined empirically for different minerals as it varies as a function of initial grain-size distribution and changes in grain-size distribution and reactive site density during dissolution/precipitation (Larsen & Postma, 2001).

The term $\left(\frac{m}{m_0} \right)^n$ thereby allows for the reaction rate to account for changes in reactive surface sites during dissolution, but it may also account for changes in crystal size, ageing of the solid or armouring of reactive surfaces (Appelo & Postma, 2005). The term $f(C)$ allows for the reaction rate to be scaled (e.g. depending on the departure from equilibrium) as a function of pH or solution composition (Lasaga, 1998).

In summary, solubilities of gypsum, anhydrite and carbonates have been investigated extensively. Nevertheless, some uncertainties remain regarding the equilibrium constants reported in the literature. Variation in the values for equilibrium constants can

result in solubility and solid-phase predictions that differ in magnitude between thermodynamic models; however, research to improve the available thermodynamic data for carbonates, gypsum and anhydrite mineral phases is ongoing (e.g. Bouchelaghem, 2010; Ruiz-Agudo *et al.*, 2015; Dai *et al.*, 2017; Voigt *et al.*, 2018). Another source of model uncertainty stems from the dependence of kinetic reaction rates on reactive surface areas. Only a small percentage of the total mineral surface area may actually participate as a reactive surface area, which is difficult to estimate with precision and is often approximated (e.g. White & Peterson, 1990). In general, however, variations in surface area of fast-reacting phases such as calcite only impact model simulations over short timescales.

Silicates

Silicates are generally considered to be relatively insoluble. At elevated temperatures, however, minor amounts of Si, Al, Mg and Fe are known to dissolve from smectite, entering the solution. Kaufhold *et al.* (2019) showed that increasing temperature leads to an increasing ratio of dissolved Si/Mg. At $<120^\circ\text{C}$, more Mg was dissolved compared to the stoichiometric dissolution (Mg dominated incongruent dissolution) and more Si was dissolved at temperatures $>120^\circ\text{C}$, suggesting that at least at such high temperatures smectites dissolve incongruently. However, the data shown in Fig. 5 suggest that at temperatures of $\sim 120^\circ\text{C}$ smectites may dissolve congruently even at circumneutral pH – or at least Mg and Si dissolve congruently. Congruent dissolution including Al and Fe, however, could not be confirmed because of the difficulties of measuring dissolved Al and Fe (explanations given by Kaufhold *et al.*, 2019). At high pH, congruent dissolution of smectites was reported by Cama *et al.* (2000). Figure 5 shows that three bentonites (B6, B11, B16) principally show the same curves despite their rather different compositions (e.g. the high Fe content of B11). The pronounced dissolution of Si from bentonite B38 can possibly be explained by a higher quartz content.

The composition of the porewater with respect to structural cations dissolved from the smectites, therefore, is supposed to be variable depending on the temperature. Smectite dissolution in large-scale tests has not been observed to date. In the ABM-1 experiment, however, the dissolution of cristobalite and clinoptilolite was observed in some contact samples. Both minerals are supposed to be less stable (more soluble) compared to feldspar, quartz or most other silicates.

The dissolution and precipitation kinetics of primary minerals such as quartz and feldspar that are present in igneous and metamorphic rocks or as detrital minerals in sedimentary rocks are generally slow. Developed rate laws commonly describe the dissolution and precipitation of primary minerals as a function of available reactive surface area and saturation state. The latter allows for the reaction rate to be scaled depending on the departure from equilibrium. The maximum rate of dissolution/precipitation occurs far from equilibrium; however, reaction kinetics slow when the solubility of the silicate mineral is being approached (Lasaga, 1998). Silicate reaction rates vary with temperature, which can be approximated using the Arrhenius equation (Rimstidt & Barnes, 1980), and they also vary with porewater composition (e.g. pH, [Al], [Mg]; e.g. Dove, 1999).

Thermodynamic data for most primary minerals exist, providing a solid base for modelling. However, it should be noted that reaction rates for silicate minerals, which have been determined in the laboratory, have generally been found to be one or more

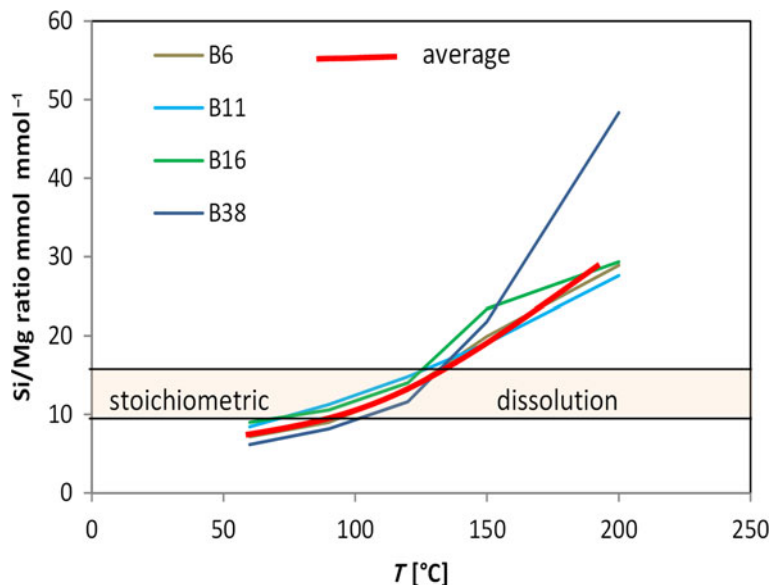


Figure 5. Si/Mg ratio of short-term smectite dissolution tests at circum-neutral pH of four different bentonites (B6, B11, B16, B38) at different temperatures. The bentonites differed with respect to their composition and cation population (Kaufhold *et al.*, 2019).

orders of magnitude faster than those observed in the field (e.g. White & Brantley, 2003; Parry *et al.*, 2015). Rate variations are attributed to differences in the composition of silicates (i.e. field reaction rates reflect the dissolution/precipitation kinetics of solid solutions rather than pure end-member minerals; Maher *et al.*, 2016), with most modelling studies adopting the simplification of treating silicates and clays as discrete end-member compositions (e.g. Wilson *et al.*, 2006b; Marty *et al.*, 2010).

Weathering of primary minerals results in the formation of secondary minerals, including smectite and other clay minerals. The variation in the composition of clay minerals such as smectite is large, and as a consequence, in contrast to primary minerals, the thermodynamic properties of smectites, which govern the stability of these minerals in solution, remain largely unresolved (Gailhanou *et al.*, 2019). May *et al.* (1986), for instance, discussed the experimental difficulties in the evaluation of dissolution

experiments of smectites. Nevertheless, smectite dissolution rates have been published by Cama *et al.* (2000), Golubev *et al.* (2006) and Rozalén *et al.* (2008); however, equilibrium achievement remains a significant issue in these solubility experiments (Blanc *et al.*, 2021). Wilson *et al.* (2006b) calculated the solubilities of different Fe-smectites and derived log(K) values that varied from -12 to 33 at 25°C, while Gailhanou *et al.* (2017) showed that hydration reactions modified the stability of smectite by >1 log(K) unit per mole of water. The large range of values probably results from ‘uncertainties associated with the thermodynamic modelling of clay mineral stability (Lippmann, 1979) and the wide variety in clay mineral composition and structure’ (Wilson *et al.*, 2006b).

Modelling codes require stability constants for the initial clay composition of the barrier system, including for smectites, as well as for any potential clay mineral end member that could form after chemical and thermal disturbances over time. With

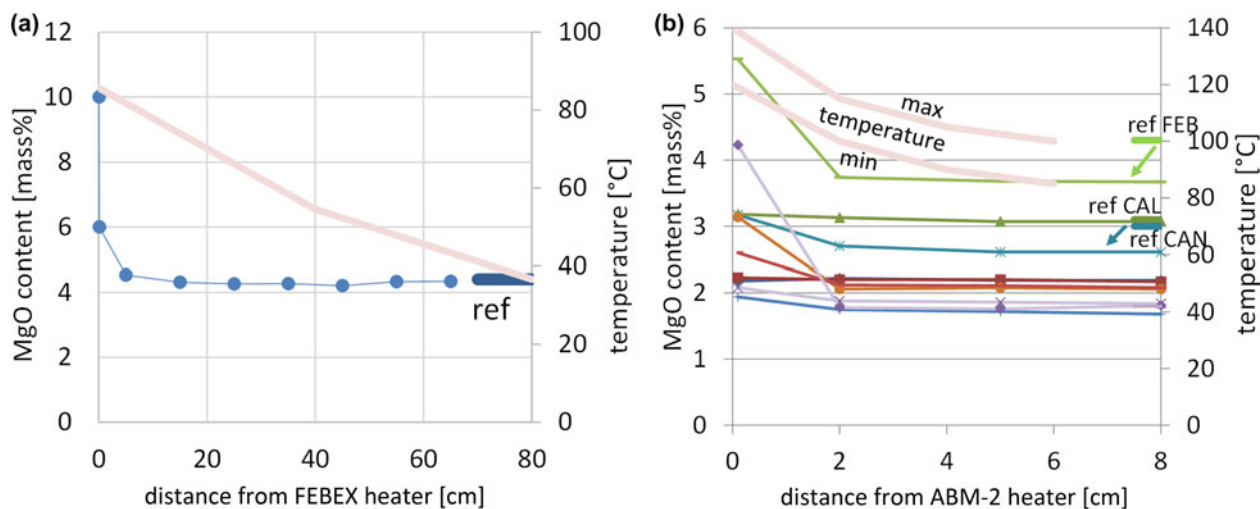


Figure 6. Example of (a) a MgO profile of the FEBEX experiment (section 54 without liner) based on Kaufhold *et al.* (2018) and (b) MgO profiles of the first 10 blocks of ABM-2 (Kaufhold *et al.*, 2017). Temperature gradients (pink) were taken from Martinez *et al.* (2016; FEBEX) and Kaufhold *et al.* (2017; ABM-2). The temperature profiles in the ABM-2 test showed some variation depending on depths. Therefore, minimum and maximum values are shown. Reference values (MgO content before the experiment) are given as bold lines assigned as ‘ref’. Higher contents of the ref materials can be explained by exchange of initially present exchangeable Mg²⁺.

few experimental data available in the literature, current practice uses estimation methods to obtain thermodynamic data in the databases of geochemical codes for clay phases whose chemical composition is known (Blanc *et al.*, 2021). Based on a limited number of experimental measurements, results are thereby extended to different clay mineral compositions to obtain thermodynamic datasets covering a larger range of clay mineralogy. Marty *et al.* (2015) simulated smectite dissolution and concluded that the major model uncertainty derived from the fact that incongruent dissolution of smectite had to be accounted for. In addition, the authors acknowledged the problem of determining the reactive surface of smectites (and other clay minerals), which is required for any kinetic modelling of their precipitation or dissolution. In addition to a reactive surface area and incongruent dissolution, smectite dissolution depends on temperature, pH and the degree of saturation of the solution. Accordingly, Alekseyev *et al.* (2007) and Marty *et al.* (2015) developed a comprehensive set of (semi-)empirical relations. This approach was also followed by Ngo *et al.* (2014), who simulated the dissolution of smectite as a function of pH, employing different kinetic constants for three distinct pH ranges: acidic, neutral and alkaline porewater conditions. These approaches provide means to consider relevant effects on the dissolution rate. However, the overall complexity of describing the dissolution of smectites introduces considerable uncertainty into current modelling studies.

In summary, modelling dissolution and precipitation of the siliceous admixtures of bentonite is less complicated compared to with smectite. Improving the understanding of smectite dissolution mechanisms hence is crucial for improving modelling of long-term barrier performance.

Mg enrichment at the heater

In most of the large-scale tests in which a contact sample was analysed, at least a slight Mg increase was observed at the heater (e.g. Fig. 6). Svensson *et al.* (2011) analysed four bentonite blocks from the ABM-1 experiment that were heated to 140°C. The authors reported that in three of the four blocks a Mg gradient had developed (increasing MgO content towards the heater). Interestingly, the Mg concentration of each of the reference materials (before the experiment started) was higher than in any of the samples taken after termination of the experiment, but no contact sample was investigated in this study. By comparing different bentonites, they could exclude dissolution of carbonates such as dolomite as the Mg source. Kaufhold *et al.* (2013) also showed that most of the nine analysed bentonite blocks exhibited Mg increases towards the heater. In ABM-2, which was heated to 140°C, 29 out of 31 bentonite blocks were sampled. The contact of most blocks showed MgO increases of >0.1 mass%, while nine blocks showed an increase of ≥ 1 mass% (first 10 blocks shown in Fig. 6b). Kumpulainen *et al.* (2016) confirmed this for two ABM-2 bentonite blocks (the block labelled FRI was not included here as that was a marine clay from Friedland, Germany).

In contrast, ABM-5, the experiment with the highest temperature of 250°C, did not exhibit a clear trend in the Mg distribution. Six blocks even showed a slight MgO decrease of >0.1 mass% towards the contact, while 15 blocks showed an increase of between 0.2 and 1.1 mass% MgO. Dohrmann & Kaufhold (2014) studied two MX80 blocks after retrieval of the prototype repository *in situ* experiment in Äspö, Sweden. They reported that exchangeable Mg in the buffer decreased (by cation exchange), while the MgO concentration had increased at the

bentonite/Cu canister interface. A uniform MgO distribution farther away from the contact can be explained by cation exchange, which may also at least partly be the source of the Mg at the heater.

It should be noted that the Mg increase towards the heater is commonly expressed as '+x% MgO' (absolute increase in mass% from the chemical analysis) and that these values depend on the area of the piece of the block used for sampling: the so-called 'contact samples' (all other samples were drilled). Commonly, 10–30 cm² are required to collect 2 g of contact sample (i.e. the amount needed for mineralogical analysis). Accordingly, the available surface area for sampling will dictate the depth of sampling, with larger surfaces available for sampling requiring a reduced sampling depth. The samples collected from the FEBEX experiment had a surface of ~ 200 cm² and therefore a reduced sampling depth (<0.1 mm; Fig. 6a; Kaufhold *et al.*, 2018). The experiment itself was conducted over 18 years, which could be an additional explanation as to why the highest Mg increase was observed in this experiment. The Mg increase was often observed, but for some materials no specific Mg-rich phase was observed (e.g. LOT experiment; Kaufhold *et al.*, 2017). In some samples from the ABM tests, however, a small increase of the d_{060} reflection of the smectite and a slight increase of the 680 cm⁻¹ infrared band were observed, which both indicate the formation of trioctahedral domains (Fig. 7). This effect has already been reported by Plötze *et al.* (2007) and Svensson (2015). Trioctahedral domains could at least theoretically form as a result of an addition reaction (Mg would enter the vacancies), or they could form as a separate trioctahedral mineral by dissolution and precipitation. Laboratory experiments showed that rather dry conditions were required to fix Mg in the vacancies (Kaufhold *et al.*, 2016). In the ABM tests, however, such dry conditions did not exist. Therefore, it is more probable that either Mg was dissolved incongruently from smectite and precipitated as a new phase near the heater or that Mg was liberated by cation exchange and migrated to the heater. In the FEBEX contact block, Kaufhold *et al.* (2018) found brucite, and Fernandez *et al.* (2018) also observed other Mg-rich silicates such as sepiolite using an electron microscope. This indicates that the Mg increase may not be triggered by a specific reaction, instead indicating that the precipitation of Mg phases is the result of Mg diffusion towards the heater caused by the thermal and hydraulic gradients. The Mg, as explained above, may be from cation exchange and/or (incongruent) dissolution of smectite. The latter would be consistent with data published by Kaufhold *et al.* (2019), who showed that the Mg/Si ratio of leached smectites depends on the temperature. The experimental data and modelling performed on Mg- and Si-oxides indicated that at temperatures <120°C more Mg is liberated by dissolution of smectites, whereas at higher temperature more Si (in relation to Mg) is liberated (Fig. 5). This could lead to a concentration gradient of Mg and Si corresponding to the respective temperature. In the colder parts more Mg would be available in solution, whereas in the hotter parts more Si would be available in solution. This could lead to migration of Mg towards the heater, where it may precipitate as a Mg-rich phase. This should, however, lead to a continuous Mg gradient inside the block. However, the Mg increase is often restricted to the contact. It also would not explain why sometimes pure Mg phases form (e.g. brucite in the FEBEX experiment). In this respect, it is interesting to note that in the case of a saponite being used in the ABM-5 test, a Mg decrease at

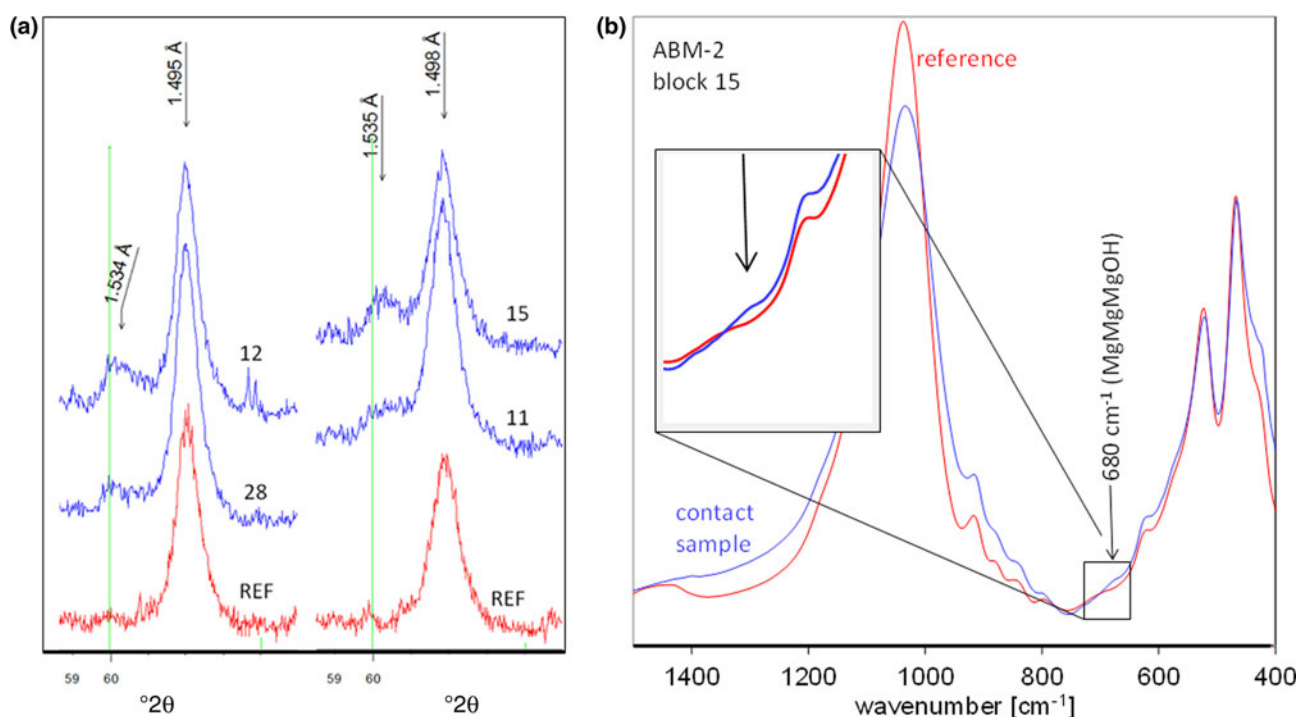


Figure 7. (a) Increase in the d_{060} intensity at ~ 1.54 Å (trioctahedral minerals) and (b) increase in the extinction of the 680 cm^{-1} infrared band, suggesting the presence of trioctahedral minerals (Kaufhold *et al.*, 2018). REF = reference.

the heater was observed (Kaufhold *et al.*, 2021). The material, of course, had a high initial Mg content (~ 16 mass% MgO).

There is a paucity of modelling studies that report on the evolution of Mg as part of bentonite buffer simulations for radioactive waste confinement. However, some studies report on alterations in Mg content in bentonites simulated on the basis of dissolution reactions. Marty *et al.* (2010) simulated long-term alterations of MX80 in contact with ambient geological fluids and a corroding steel canister, and they observed the dissolution of montmorillonite, which in turn resulted in elevated Mg pore-water concentrations. Similarly, Savage *et al.* (2010) modelled Mg release from dissolving Ca-montmorillonite as part of the long-term geochemical changes of a bentonite buffer in contact with a steel canister. Subsequently, dolomite, as an Mg-rich calcium carbonate, was simulated to precipitate in proximity to the iron canister/bentonite interface. It is conceivable that bentonite dissolution and subsequent diffusion of Mg and/or thermal-induced migration towards the heater (Jodin-Caumon *et al.*, 2012) could lead to Mg enrichment; however, to the knowledge of the authors, this process has not been described as part of a model study to date. The possibility of predicting this reaction would largely depend on the accuracy with which smectite dissolution, including incongruent Mg dissolution from smectite, could be described as a function of temperature.

Illitization

The reaction of smectites with K^+ is frequently investigated because the oil industry uses the parameter 'illite crystallinity' or 'Kübler index' to obtain information about the burial history of sediments, which in turn is important with respect to the formation of oil and gas in the deeper sediments. The basic idea behind progressive illitization is that the marine sediments, as they settled on the sea floor, contain smectite, amongst other

minerals. The burial history of such marine clays starts as the amount of overlying sediment increases. The increasing load leads to compaction and the formation of a claystone or shale. With increasing temperature and time, the organic matter matures, and at certain points it forms oil and gas. Such maturation sequences are observed in basins containing marine clays. The maturity of the organic material can be correlated with the amount of illite that formed in relation to the starting material. Illitization, therefore, results from increased pressure, temperature and time, but it also depends on the availability of K^+ in the basins. Without the presence of K^+ , smectite is preserved despite significant overload for several hundreds of millions of years, and hence illitization can be considered slow compared with the lifetime of a repository (Sellin & Leupin, 2013). The reaction of smectite and K^+ is special because K^+ can be fixed in the ditrigonal holes of the tetrahedral sheet (because of its diameter and low hydration energy; Lagaly, 1993) and because it can induce the formation of illite (Kaufhold & Dohrmann, 2010b). To date, two conceptual models are considered that could explain illitization: solid-state transformation (Hower *et al.*, 1976) and dissolution and precipitation (Boles & Franks, 1979).

The simplest pathway for conversion of smectite into a 10 Å phase would be to exchange the exchangeable cations by K^+ followed by drying to remove the hydration water of K^+ . The resulting 10 Å peak in XRD is often misinterpreted as illite. In fact, this peak corresponds to a 2:1 layer silicate with a dehydrated interlayer but not necessarily illite, which is distinguished from smectite based on its layer charge density ($0.6\text{--}0.9\text{ eq FU}^{-1}$ instead of $0.2\text{--}0.6\text{ eq FU}^{-1}$ for smectites) and the extent of Si-by-Al substitution in the tetrahedral sheet.

Illitization has been investigated in several laboratory studies (Eberl, 1978; Güven & Huang, 1991; Herbert *et al.*, 2004; Hofmann *et al.*, 2004; Suzuki *et al.*, 2008). Kaufhold & Dohrmann (2010b) reacted different bentonites with KCl

solutions and could distinguish different phases: real illite (no H₂O swelling (= zero-water-layer state) and no cation exchange from the interlayer region), K⁺-exchanged smectite 1 (no H₂O swelling (= zero-water-layer state) but exchangeable K⁺ from the interlayer region) and K⁺-smectite 2 (hydratable and exchangeable K⁺ from the interlayer region). Through XRD analysis and measuring under 'air-dry' conditions and with ethylene glycol (EG) solvation, one could distinguish even more phases. In most studies in which significant formation of real illite was observed, chemicals were added supporting the dissolution of smectite, such as KOH (Bauer & Velde, 1999) or organic acids (Schlosser *et al.*, 2019), indicating that smectite dissolution is important with respect to illitization. Notably, the water/solid ratios were much larger compared to repository conditions, which would have accelerated illitization in these experiments.

According to the model provided by Kaufhold & Dohrmann (2010b), real illite forms if K⁺, Al and Si are present in solution. In a system with excess water containing K⁺, smectite (depending on temperature) partly dissolves (most likely only small percentage), providing some Al and Si within the solution. If K⁺ is present, illite precipitates, leaving some silica in solution, which is a byproduct of real illitization ('real' means that the actual crystal chemical process occurred, not just a collapse of the interlayer region). As a result of illite precipitation, the solution is depleted in Al and Si, and smectite dissolution can proceed as described above. Illite and SiO₂ precipitate as long as excess K⁺ is available in solution. The entire process of illitization, therefore, is supposed to depend on K⁺ availability, which is supposed to be restricted to the K⁺ introduced to the EBS by inflowing water (i.e. K⁺ availability would depend on the composition of the surrounding water). It should be noted that illitization is slower than cation-exchange reactions and is therefore probably not observable in any EBS from the beginning of its activity. However, at both the bentonite/cement and at the bentonite/iron interface the solubility of the smectite is significantly increased under high pH (cement porewater) and due to reductive dissolution (low Eh at the Fe canister), which could also lead to illitization if K⁺ was present.

Important information regarding illitization can be gained from natural analogue studies because the process of illitization is rather slow. In natural analogue studies in Kinnekulle, Sweden, Pusch (1983) and Brusewitz (1986) studied the influence of heat on the loss of swelling capacity due to illitization and the release of free silica by observing mineralogical changes following an intrusion into Ordovician bentonite layers. The authors demonstrated that temperatures exceeded 100°C and that the resulting heat plume influenced the bentonite layer for several hundreds of years. Pusch (1983) suggested that '[a] possible cementation mechanism, i.e. that of quartz precipitation, is very probably associated with the smectite/illite conversion'. This was concluded due to the fact that SiO₂ forms upon real illitization. The authors speculated that such silica cementation could reduce the swelling capacity of the barrier, in addition to the loss of swelling capacity caused by smectite transformation. Müller-Vonmoos *et al.* (1990, 1994) critically assessed this hypothesis; however, the authors could not distinguish between potentially large amounts of free silica from the devitrification of volcanic ash and relatively low amounts of free silica from illitization. Sauer *et al.* (2020) performed hydrothermal experiments with mixtures of Opalinus Clay and Wyoming bentonite up to 300°C for 6 weeks and also could not identify illitization experimentally. Cheshire *et al.* (2014) studied the alteration of Wyoming bentonite in

hydrothermal experiments but concluded that '[t]here was no evidence of illite–smectite mixed-layering from any of the experiments conducted in this investigation'. Instead, K⁺ was exchanged in the montmorillonite interlayer.

Several studies have attempted to quantify illitization by using semi-empirical kinetic models, with rate expressions defined either on the basis of observed mineral transformations as part of burial diagenesis or through laboratory data (e.g. Eberl & Hower, 1976; Pytte, 1982; Velde & Vasseur, 1992; Huang *et al.*, 1993). Karnland & Birgersson (2006) compared two laboratory-based models proposed by Huang *et al.* (1993) and Cuadros & Linares (1996), as well as a field-based kinetic rate expression proposed by Pytte & Reynolds (1989), for their ability to quantify illitization as part of the KBS-3 repository concept. The model by Huang *et al.* (1993) was regarded to be most suitable, as the applied kinetic rate expression and its associated parameters are based on laboratory work and as the model was tested independently on geological settings with reasonable agreement. The Huang *et al.* (1993) model considers a temperature dependence of the illitization rate based on an Arrhenius type expression; it also considers the montmorillonite fraction and potassium concentration, but it does not include parameters such as pH, water content and thermal gradient (see Equation 3):

$$\frac{dS}{dt} = -8.1 \times 10^4 \times e^{\frac{-14,100}{T}} \times [K^+] \times S^2 \quad (3)$$

where dS/dt is the illitization rate, $[K^+]$ is the potassium ion concentration, S the smectite fraction and T the absolute temperature in Kelvin.

All models, however, agree that illitization will be relatively slow in the bentonite barrier and hence probably of less relevance compared to other reactions. Illitization has also been inferred by several numerical geochemical modelling studies. Zheng *et al.* (2015, 2017) used coupled thermal, hydraulic, mechanical and chemical modelling to simulate a bentonite-backfilled EBS system in a clay formation over 1000 years and over 100,000 years. In both studies, two temperature scenarios were considered: a case in which the temperature in the bentonite near the waste canister peaked at 100°C; and another in which the temperature was allowed to reach 200°C. Illitization was simulated as a dissolution/precipitation reaction. Smectite was allowed to dissolve under the formation of illite, with the illitization rate calibrated against field data. Both studies showed illitization to occur in the bentonites as well as in the clay formation, being enhanced under higher temperatures. Illitization resulted in a notable reduction in the swelling stress of the employed bentonites. However, the model results were not verified experimentally. Approximating illitization through a dissolution/precipitation reaction was also undertaken by Savage *et al.* (2020), simulating the burial of marine sediments over geological timeframes and increasing temperatures. The smectite fraction within the sediment was included as a K-montmorillonite, with both illite and smectite modelled as discrete minerals rather than mixed layers. The rate and magnitude of illitization predicted by the model was verified against the observed mineralogical data, with depth determined from a site offshore of Japan. It was found that the onset of illitization of smectite with depth, time and temperature from the model was able to be matched with previous data, but the overall rate of transformation was much more rapid in the model compared to the observed mineralogical data.

Geochemical modelling of illitization requires thermodynamic data for illite/smectite and any mixed-layer minerals; however, the thermodynamic stability of illite/smectite mixed-layer minerals remains an unsolved issue due to the inherent non-stoichiometric nature of these minerals (Gailhanou *et al.*, 2012, 2019). As a consequence, modelling studies generally adopt an idealized stoichiometry, which will introduce uncertainties with regards to mineral stability. The lack of a larger set of thermodynamic data representing a range of mineral compositions remains a limitation for predicting illitization rates as part of numerical long-term performance assessments of radioactive waste repository concepts.

To date, investigation of illitization remains an analytical challenge, mostly because illitization leads to the formation of mixed-layer minerals, which, from an analytical point of view, represent the most challenging of clay minerals. Important studies regarding the structural aspects of illitization, which are not discussed further in this study, have been published by Honty *et al.* (2004) and Meunier & Velde (2004).

Mineral alteration at the bentonite/iron interface

The formation of corrosion phases at the contact with an Fe heater (or carbon steel) and the formation of secondary silicates at the cement/bentonite interface may not be considered as thermally induced reactions because they also happen at room temperature, sometimes occurring even more rapidly (Stoullil *et al.*, 2013). The effect of temperature on the mechanism and/or extent of these interface reactions is rarely considered in a systematic manner. Stoullil *et al.* (2013) reported a slightly lower corrosion rate at 90°C compared to 40°C, which the authors explained by a denser magnetite layer in cases of higher temperatures, leading to less Fe²⁺ diffusion. Both interface reactions (bentonite/iron and bentonite/cement) are affected but not exclusively triggered by temperature. Therefore, they are discussed briefly in the following. The large number of studies conducted on the reactions dealing with these interfaces justify a separate review. Hence, only a couple of studies are cited below.

The bentonite/copper interface is considered to be relatively inert as long as sulfides are absent. The reaction of bentonite and metallic iron (or carbon steel), however, leads to the formation of different corrosion products. Commonly, magnetite and Fe-silicates are observed. At low temperatures, 1:1 Fe-silicates ('7 Å phases') form, which were characterized in detail by Lanson *et al.* (2012). High-temperature experiments (i.e. >150°C) often resulted in the formation of chlorites ('14 Å phases'; Guillaume *et al.*, 2003; Wersin *et al.*, 2013; Zandanel *et al.*, 2022), sometimes accompanied by zeolites and even Fe-smectite. Apart from the identification and characterization of corrosion products, the reaction mechanism has also been investigated (Kaufhold *et al.*, 2020b). Firstly, Fe corrosion leads to the formation of hydrogen, which in turn reduces structural ferric iron in the smectites (both at room temperature or elevated temperatures). Based on this reaction, the bentonite has to be understood as an Eh buffer. Indeed, Gorski *et al.* (2013) showed a correlation between Eh and layer charge density, and Kaufhold *et al.* (2015) were able to show a correlation between corrosion rate and layer charge density. Gorski *et al.* (2013) argue that these correlations are a consequence of low-charge smectites being more oxidizing than high-charged smectite, which, in turn, explains the higher corrosion rates of low-charge smectites (or bentonites containing low-charge smectites). The different

extents of corrosion at the Fe interface of different bentonites can be understood based on the reducibility of structural Fe³⁺. In other words, different smectites require different H₂ concentrations at which significant Fe³⁺ reduction starts. Quantifying corrosion rates within a numerical model would therefore require an understanding of the Eh buffering capacity of different smectites. As a result of the reduction of structural Fe³⁺, smectites become less stable and hence more soluble. This increased solubility is referred to as 'reductive dissolution' (Jaisi *et al.*, 2005). It leads to the formation of Fe-silicates, but the presence of carbonates may additionally and/or alternatively lead to the formation of Fe-carbonates. The rate of formation of Fe-silicates should, therefore, be faster than expected based on regular smectite dissolution rates.

Consistent results were reported on the corrosion rate ranging from 1 to 5 µm year⁻¹ (Foct & Gras, 2003; Bildstein *et al.*, 2006; Savage *et al.*, 2010; Stoullil *et al.*, 2013; Smart *et al.*, 2017; Chaparro *et al.*, 2021). For empirical modelling, it is therefore feasible to use an average value or maximum and minimum values. A number of modelling studies have been undertaken on iron-bentonite interactions, with most studies assuming fully anoxic conditions over the duration of the model time, disregarding the initial period of oxygen consumption given its short duration (e.g. Marty *et al.*, 2010). Accordingly, corrosion of iron/steel containers is generally simulated as an anaerobic reaction, assuming that sufficient water is available to maintain a continuous redox reaction. Frequently, corrosion rates are simulated as constant over time (1–5 µm year⁻¹). Some authors, however, have introduced kinetic corrosion rates. Samper *et al.* (2016), who simulated the interactions of corrosion products and compacted bentonite over 1 million years, took the thermal gradient across the bentonite buffer into account, as well as the temperature dependence of the corrosion rate. Their results suggest that the initial corrosion rate increases from 2.00 to 4.75 µm year⁻¹ and then decreases after 10,000 years to ~2.2 µm year⁻¹. The authors found that the temperature dependence of the corrosion rate did not result in any significant influence on the geochemical evolution of the bentonite buffer over the longer term. Others employed kinetic corrosion rates with a rate dependence on the dissolved Fe²⁺ concentration (e.g. Marty *et al.*, 2010; Lu *et al.*, 2011). It is noteworthy that this led to a significant reduction in the maximum corrosion rate of the simulated canisters to <1 µm year⁻¹. Similarly, Wilson *et al.* (2015) simulated kinetic corrosion with the rate limited by the diffusive supply of hydrogen to the iron/steel surface. This also led to a significant reduction in anaerobic steel corrosion (0.06 µm year⁻¹) compared to the static corrosion rates.

The production of hydrogen gas as part of canister corrosion and its implications for the integrity of the bentonite barrier are not well understood at present, and, accordingly, modelling approaches diverge. Although Xu *et al.* (2008) explicitly simulated H₂ gas generation and the associated pressure build-up, showing that gas pressure build-up was strongly correlated with the assumed corrosion rate, many modelling studies do not consider vapour phases and simulate the bentonite barrier as a fully water-saturated system. In these models, corrosion products such as Fe²⁺ are released along with hydrogen, which migrate through the clay barrier by diffusion (Montes *et al.*, 2005; Samper *et al.*, 2008; Marty *et al.*, 2010; Ngo *et al.*, 2014; Wilson *et al.*, 2015). In essence, these models simulate the reaction of bentonite with corrosion product-equilibrated water rather than simulating a physical contact between bentonite and a steel canister.

The transformations of primary bentonite minerals in the near field of a spent-fuel Fe/steel canister are simulated to produce Fe²⁺-rich alteration products. However, model assumptions such as the secondary minerals included in the model, the kinetic rate laws employed, the reactive surface areas assumed, the thermodynamic database used and whether isothermal conditions or the evolution of the temperature is considered result in variations in the simulated bentonite alterations. Wilson *et al.* (2015) simulated Fe²⁺-rich clays as the products of direct contact between bentonite and the steel canister. Similarly, Chaparro *et al.* (2021) predicted Fe-silicate phases (greenalite, nontronite) as corrosion products together with magnetite. Others have simulated magnetite and siderite as the main steel corrosion products at the interface with compacted bentonite (Samper *et al.*, 2008; Lu *et al.*, 2011; Samper *et al.*, 2016), aluminosilicates such as Fe–Al-chlorite and Mg–Al-chlorite (Marty *et al.*, 2010; Ngo *et al.*, 2014) and serpentine-like minerals such as berthierine, cronstedtite and chamosite (Bildstein *et al.*, 2006). Savage *et al.* (2010) concluded that more data on Fe-silicates are needed to improve Fe-bentonite modelling. The effect of layer charge density on the reducibility and hence solubility of smectites explained above has not yet been included in geochemical modelling of bentonite/iron interactions, which would explain why Fe-silicates are hardly predicted by modelling (as in the NF-PRO project; Arcos *et al.*, 2008).

In summary, different corrosion products were identified at the iron/bentonite interface. Most commonly, magnetite is sometimes found directly at the heater (not necessarily), followed by a Fe-silicate layer (7 Å or 14 Å depending on the temperature). The corrosion rate was consistently reported to range from 1 to 5 µm year⁻¹. The entire system is not yet fully understood in terms of the effects of different bentonite components (opals, carbonates, interlayer compositions, etc.) on the corrosion rate and the formation of different corrosion products at different temperatures. Systematic studies are lacking, which should be accompanied by modelling to improve the available thermodynamic data, particularly those regarding the potential Fe-rich siliceous corrosion products listed above.

Mineral alteration at the bentonite/cement interface

As explained in the previous section, neither reaction – iron/bentonite nor cement/bentonite – is thermally induced. Nevertheless, a large number of publications are available on both reactions due

to their relevance for the integrity of EBS systems and due to their complexity. A recent and comprehensive summary of studies on the bentonite/cement interaction was published by Wieland *et al.* (2017). In the present paper, therefore, only brief summaries of the reaction and approaches to modelling it are provided.

The cement/bentonite interface may not exist in all EBS concepts, but the topic was and is investigated extensively (Oda *et al.*, 2004; Gaucher *et al.*, 2006; Savage *et al.*, 2007). In addition, the temperature may be lower at the bentonite/cement interface compared with the canister/bentonite interface, as cement plugs (or similar), which are used to seal shafts, will be farther away from the canisters. The cement porewater of ordinary Portland cement is known to be alkaline due to hydrolysis, mainly of Ca-oxide. The alkaline solutions significantly facilitate the dissolution of smectites, and, depending on the chemical composition of the smectite and possible minor phases, different alteration products form (e.g. Yokoyama *et al.*, 2021). Sawaguchi *et al.* (2016) reported on high-pH alteration experiments with Kunipia-F bentonite, with a focus on dissolution of montmorillonite at elevated temperatures (50–90°C) in relation to the activity of OH⁻. Differences in dissolution rates of montmorillonite were explained by considering OH⁻ activity accompanied by the dissolution of accessory minerals such as quartz and chalcedony. Recent summaries of both experimental and modelling approaches have been provided by Wieland *et al.* (2017) and Jacques *et al.* (2021). Kaufhold *et al.* (2020a) investigated the cement/bentonite interface based on mixing powders, which allowed for the application of bulk analysis as a representative of the interfaces. They showed that the degree to which smectite is dissolved depends on the amount of reactive silica that is present in bentonites (e.g. as opal-A). The experimental data confirmed previous modelling of this buffered reaction by Arthur & Savage (2016). The thermodynamic data regarding the possible alteration products such as sulphates, carbonates, feldspar and zeolites are considered to be more accurate than those for smectite. Successful modelling of these reactions may also result from the fact that smectites dissolve congruently at high pH, which is more straightforward to simulate than incongruent dissolution.

Systematic data regarding temperature effects concerning the cement/bentonite reaction are available (Fig. 8). Kaufhold *et al.* (2020a) varied the temperature of bentonite/cement/water mixtures from 30°C to 80°C (although the temperature at the bentonite/cement interface in a real repository may be well below 80°C because of its larger distance from the canister). The results

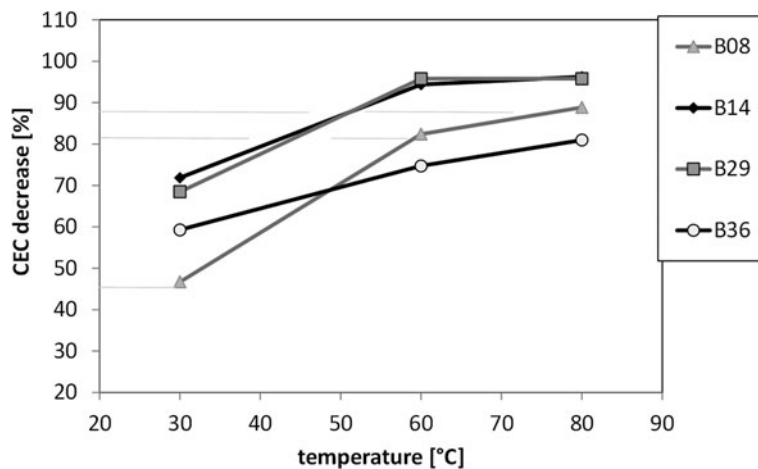


Figure 8. Extent to which smectites are dissolved in contact with cement depending on the temperature (Kaufhold *et al.*, 2020a).

were evaluated based on a comparison of CEC data at different temperatures, which were shown to correspond to the extent of smectite degradation. Some bentonites showed significant increases in the extent of smectite degradation between 30°C and 60°C (e.g. increase from 45% to 80%), but less so between 60°C and 80°C (+5%), whereas other bentonite blocks showed an almost linear slope.

In summary, the reaction of bentonite with cement is driven by the dissolution of smectite and the precipitation of secondary phases, with the type depending on the chemical composition. Because of the high pH, smectite dissolution is presumably congruent, which is advantageous with respect to numerical modelling.

Conclusions

Many of the mineralogy-related reactions observed in bentonite barrier systems were summarized and discussed, highlighting long-term, large-scale and laboratory experiments. As the relevant phenomena are essentially all influenced by temperature and most large-scale experiments are conducted at elevated temperatures, a clear emphasis was placed on the temperature dependence of the respective phenomena.

The long-term safety assessment of barrier systems has to rely on numerical modelling. To arrive at realistic model predictions, all relevant reactions need to be identified and reasonable input parameters have to be established. Given the complexity of a barrier system and the multitude of phenomena that occur in such a setting, this is certainly a stepwise process.

From the discussion of the dissolution of the main bentonite components, it appears that the (temperature-dependent) dissolution of smectites deserves more attention. This is especially evident when considering the increase in magnesium concentrations close to heaters, which could be ascribed to incongruent dissolution. Considering the dissolution of smectites at bentonite/cement interfaces, the situation might be less complicated because, due to comparatively high pH values, the smectite could be assumed to dissolve congruently. A further difficulty can be expected at the interface of bentonite and iron/steel, where, as a result of the reduction of structural iron, reductive dissolution of smectites may occur. These processes, together with ion-exchange equilibria at elevated temperatures driven by changes in groundwater composition, can be expected to impact the long-term safety assessment of barrier systems and deserve further attention.

Acknowledgements. The present review was motivated by the HotBent Team (project head: Dr Florian Kober), who requested of us to summarize the challenges of modelling thermally induced reactions in bentonite buffers.

References

- Alekseyev V.A. (2007) Equations for the dissolution reaction rates of montmorillonite, illite, and chlorite. *Geochemistry International*, **45**, 770–780.
- Amos R.T., Blowes D.W., Bailey B.L., Sego D.C., Smith L. & Ritchie A.I.M. (2015) Waste-rock hydrogeology and geochemistry. *Applied Geochemistry*, **57**, 140–156.
- Appelo C. & Postma D. (2005) *Geochemistry, Groundwater and Pollution*, 2nd edition. Balkema, Rotterdam, The Netherlands, 683 pp.
- Appelo C.A.J., Verweij E. & Schäfer H. (1998) A hydrogeochemical transport model for an oxidation experiment with pyrite/calcite/exchangers/organic matter containing sand. *Applied Geochemistry*, **13**, 257–268.
- Arcos D, Bruno J, Benbow S. & Takase H. (2000) *Behaviour of Bentonite Accessory Minerals during the Thermal Stage*. SKB Technical Report TR-00-06. Svensk Kärnbränslehantering AB, Stockholm, Sweden, 52 pp.
- Arcos D., Cuevas J., Fernández A.M., Herbert H.-J., Hernan P., Van Loon L. et al. (2008) Key processes affecting the chemical evolution of the engineered barrier system. Pp. 183–192 in: *NF-PRO Project, Conference Paper Euradwaste 08: Seventh European Commission Conference on the Management and Disposal of Radioactive Waste*. Publications Office of the European Union, Luxembourg.
- Arthur R. & Savage D. (2016) *Long-Term Stability of Clay Minerals in the Buffer and Backfill*. STUK-TR 22. STUK, Helsinki, Finland, 31 pp.
- Assad F.F., Sabet V.M. & Srivastava S.N. (1981) Thermodynamics of Na-Ca ion exchange clay soil system. *Zeitschrift für Physikalische Chemie*, **262**, 525–532.
- Baborová L., Vopálka D. & Červinka R. (2018) Sorption of Sr and Cs onto Czech natural bentonite: experiments and modelling. *Journal of Radioanalytical and Nuclear Chemistry*, **318**, 2257–2262.
- Bauer A. & Velde B. (1999) Smectite transformation in high molar KOH solutions. *Clay Minerals*, **34**, 259–273.
- Bildstein O., Trotignon L., Perronnet M. & Jullien M. (2006) Modelling iron-clay interactions in deep geological disposal conditions. *Physics and Chemistry of the Earth, Parts A/B/C*, **31**, 618–625.
- Bingham J.M. & Nordstrom D.K. (2000) Iron and aluminum hydroxysulfates from acid sulfate waters. *Reviews in Mineralogy and Geochemistry*, **40**, 351–403.
- Blanc P., Gherardi F., Vieillard P., Marty N.C.M., Gailhanou H., Gaboreau S. et al. (2021) Thermodynamics for clay minerals: calculation tools and application to the case of illite/smectite interstratified minerals. *Applied Geochemistry*, **130**, 104986.
- Boles J.R. & Franks S.G. (1979) Clay diagenesis in Wilcox sandstones of southwest Texas: implications of smectite diagenesis on sandstone cementation. *Journal of Sedimentary Petrology*, **49**, 55.
- Bouchelaghem F. (2010) A numerical and analytical study on calcite dissolution and gypsum precipitation. *Applied Mathematical Modelling*, **34**, 467–480.
- Bradbury M.H. & Baeyens B. (2000) A generalised sorption model for the concentration dependent uptake of caesium by argillaceous rocks. *Journal of Contaminant Hydrology*, **42**, 141–163.
- Bruggenwert M.G.M. & Kamphorst A. (1981) Survey of experimental information on cation exchange in soil systems. Pp. 141–203 in: *Soil Chemistry B. Physico-Chemical Models*, 2nd edition (G.H. Bolt, editor), Vol. 5, part B of *Developments in Soil Science*. Elsevier, Amsterdam, The Netherlands.
- Brusewitz A.M. (1986) Chemical and physical properties of Palaeozoic potassium bentonites from Kinnekulle, Sweden. *Clays and Clay Minerals*, **34**, 442–454.
- Cama J., Ganor J., Ayora C. & Lasaga C.A. (2000) Smectite dissolution kinetics at 80°C and pH 8.8. *Geochimica et Cosmochimica Acta*, **64**, 2701–2717.
- Carlsson L., Karnland O., Rance A., Smart N.R., Snellman M., Vähänen M. & Werme L.O. (2008) *Experimental Studies of the Interactions between Anaerobically Corroding Iron and Bentonite*. SKB Report R-08-28. Svensk Kärnbränslehantering AB, Stockholm, Sweden, 63 pp.
- Chaparro M.C., Finck N., Metz V. & Geckeis H. (2021) Reactive transport modelling of the long-term interaction between carbon steel and MX-80 bentonite at 25 °C. *Minerals*, **11**, 1272.
- Cherif M.A., Martin-Garin A., Gérard F. & Bildstein O. (2017) A robust and parsimonious model for caesium sorption on clay minerals and natural clay minerals. *Applied Geochemistry*, **87**, 22–37.
- Cheshire M.C., Caporuscio F.A., Rearick M.S., Jove-Colon C. & McCarney M.K. (2014) Bentonite evolution at elevated pressures and temperatures: an experimental study for generic nuclear repository designs. *American Mineralogist*, **99**, 1662–1675.
- Christidis G., Chryssikos G.D., Derkowski A., Dohrmann R., Eberl D.D., Joussein E. & Kaufhold S. (2023) Methods for determination of the layer charge of smectites. *Clays & Clay Minerals*, **71**, 25–53.
- Cuadros J. & Linares J. (1996) Experimental kinetic study of the smectite-to-illite transformation. *Geochimica et Cosmochimica Acta*, **60**, 439–453.

- Dai Z., Kan A.T., Shi W., Zhang N., Zhang F., Yan F. et al. (2017) Solubility measurements and predictions of gypsum, anhydrite, and calcite over wide ranges of temperature, pressure, and ionic strength with mixed electrolytes. *Rock Mechanics and Rock Engineering*, **50**, 327–339.
- Davis G.B. & Ritchie A.I.M. (1986) A model of oxidation in pyritic mine wastes 1 – equations and approximate solution. *Applied Mathematical Modelling*, **10**, 314–322.
- Deguedre C. (1994) *Colloid Properties in Groundwater from Crystalline Formations*. Nagra Technical Report, NTB 92-05. Nagra, Wettingen, Switzerland, 107 pp.
- Dohrmann R. & Kauffhold S. (2014) Cation exchange and mineral reactions observed in MX80 buffer samples of the prototype repository in situ experiment in Äspö, Sweden. *Clays and Clay Minerals*, **62**, 357–373.
- Dohrmann R. & Kauffhold S. (2017) Characterization of the second package of the alternative buffer material (ABM) experiment – II exchangeable cation population rearrangement. *Clays and Clay Minerals*, **65**, 104–121.
- Dohrmann R., Kauffhold S. & Lundqvist B. (2013a) The role of clays for safe storage of nuclear waste. Pp. 677–710 in: *Developments in Clay Science, Vol. 5B, Handbook of Clay Science, Techniques and Applications* (F. Bergaya and G. Lagaly, editors). Elsevier, Amsterdam, The Netherlands.
- Dohrmann R., Olsson S., Kauffhold S. & Sellin P. (2013b) Mineralogical investigations of the first package of the alternative buffer material test II. Exchangeable cation population rearrangement. *Clay Minerals*, **48**, 215–233.
- Dos Santos E.C., de Mendonça Silva J.C. & Duarte H.A. (2016) Pyrite oxidation mechanism by oxygen in aqueous medium. *Journal of Physical Chemistry C*, **120**, 2760–2768.
- Doula M., Ioannou A. & Dimirkou A. (1995) Thermodynamics of potassium exchange in calcium bentonite (Ca-b). *Communications in Soil Science and Plant Analysis*, **26**, 1535–1545.
- Dove P.M. (1999) The dissolution kinetics of quartz in aqueous mixed cation solutions. *Geochimica et Cosmochimica Acta*, **63**, 3715–3727.
- Eberl D. (1978) The reaction of montmorillonite to mixed-layer clay: the effect of interlayer alkali and alkaline earth cations. *Geochimica et Cosmochimica Acta*, **42**, 17.
- Eberl D. & Hower J. (1976) Kinetics of illite formation. *Geological Society of America Bulletin*, **87**, 1326–1330.
- Eberl D. & Hower J. (1977) The hydrothermal transformation of sodium and potassium smectite into mixed-layer clay. *Clays and Clay Minerals*, **25**, 215–227.
- Eckert P. & Appelo C.A.J. (2002) Hydrogeochemical modeling of enhanced benzene, toluene, ethylbenzene, xylene (BTEX) remediation with nitrate. *Water Resources Research*, **38**, 1130.
- Elberling B., Nicholson R.V. & Scherer J.M. (1994) A combined kinetic and diffusion model for pyrite oxidation in tailings: a change in controls with time. *Journal of Hydrology*, **57**, 47–60.
- Endell J. (1939) Die Abhängigkeit des Kationenaustausches und der Quellung bei Montmorillonit von der Vorerhitzung. PhD study university Rostock, *Angewandte Chemie*, **52**, 708–718.
- Fakhreddine S., Lee J., Kitanidis P.K., Fendorf S. & Rolle M. (2016) Imaging geochemical heterogeneities using inverse reactive transport modeling: an example relevant for characterizing arsenic mobilization and distribution. *Advances in Water Resources*, **88**, 186–197.
- Feng J., Tian H., Huang Y., Ding Z. & Yin Z. (2019) Pyrite oxidation mechanism in aqueous medium. *Journal of the Chinese Chemical Society*, **66**, 345–354.
- Fernández A.M., Kauffhold S., Sánchez-Ledesmaa D.M., Reya J.J., Melóna A., Robredo L.M. et al. (2018) Evolution of the THC conditions in the FEBEX *in situ* test after 18 years of experiment: smectite crystallochemical modifications after interactions of the bentonite with a C-steel heater at 100 °C. *Applied Geochemistry*, **98**, 152–171.
- Ferrage E., Sakharov B.A., Michot L.J., Delville A., Bauer A., Lanson B. et al. (2011) Hydration properties and interlayer organization of water and ions in synthetic Na-smectite with tetrahedral layer charge. Part 2. Toward a precise coupling between molecular simulations and diffraction data. *Journal of Physical Chemistry C*, **115**, 1867–1881.
- Foct F. & Gras J.-M. (2003) Semi-empirical model for carbon steel corrosion in long term geological nuclear waste disposal. Pp. 92–102 in: *Prediction of Long Term Corrosion Behaviour in Nuclear Waste Systems* (Ferron D. & McDonald D.D., editors). European Federation of Corrosion.
- Fuller A.J., Shaw S., Peacock C.L., Trivedi D., Small J.S., Abrahamson L.G. & Burke I.T. (2014) Ionic strength and pH dependent multi-site sorption of Cs onto a micaceous aquifer sediment. *Applied Geochemistry*, **40**, 32–42.
- Gailhanou P., Blanc J.R., Mikaelian G., Kawaji H., Olives J., Amouric M. et al. (2012) Thermodynamic properties of illite, smectite and beidellite by calorimetric methods: enthalpies of formation, heat capacities, entropies and Gibbs free energies of formation. *Geochimica et Cosmochimica Acta*, **89**, 279–301.
- Gailhanou H., Vieillard P., Blanc P., Lassin A., Denoyel R., Bloch E. et al. (2017) Methodology for determining the thermodynamic properties of smectite hydration. *Applied Geochemistry*, **82**, 146–163.
- Gailhanou H., Blanc P., Rogez J., Mikaelian G., Kawaji H., Olives J. et al. (2019) Thermodynamic properties of mixed-layer illite-smectite by calorimetric methods: acquisition of the enthalpies of mixing of illite and smectite layers. *Journal of Chemical Thermodynamics*, **138**, 78–97.
- Gaucher E.C. & Blanc P. (2006) Cement/clay interactions – a review: experiments, natural analogues, and modeling. *Waste Management*, **26**, 778–788.
- Golubev S.V., Bauer A. & Pokrovsky O.S. (2006) Effect of pH and organic ligands on the kinetics of smectite dissolution at 25°C. *Geochimica et Cosmochimica Acta*, **70**, 4436–4451.
- Gorski C.A., Klüpfel L.E., Voegelin A., Sander M. & Hofstetter T.B. (2013) Redox properties of structural Fe in clay minerals: 3. Relationships between smectite redox and structural properties. *Environmental Science & Technology*, **47**, 13477–13485.
- Greenberg H.R., Wen J. & Buscheck T.A. (2013) *Scoping Thermal Analysis of Alternative Dual-Purpose Canister Disposal Concepts*. LLNL-TR-639869 Lawrence Livermore National Laboratory report. Retrieved from https://digital.library.unt.edu/ark:/67531/metadc837426/m2/1/high_res_d/1090011.pdf
- Gregory D.D., Lyons T.W., Large R.R., Jiang G., Stepanov A.S., Diamond C.W., Figueroa M.C. & Olin P. (2017) Whole rock and discrete pyrite geochemistry as complementary tracers of ancient ocean chemistry: An example from the Neoproterozoic Doushantuo Formation, China. *Geochimica et Cosmochimica Acta*, **216**, 201–220.
- Gu B.X., Wang L.M., Minc L.D. & Ewing R.C. (2001) Temperature effects on the radiation stability and ion exchange capacities of smectite. *Journal of Nuclear Materials*, **297**, 345–354.
- Guillaume D., Neaman A., Cathelineau M., Mosser-Ruck R., Peiffert C., Abdelmoula M. et al. (2003) Experimental synthesis of chlorite from smectite at 300°C in the presence of metallic Fe. *Clay Minerals*, **38**, 281–302.
- Güven N. & Huang W.L. (1991) Effect of octahedral Mg²⁺ and Fe³⁺ substitution on hydrothermal illitization reactions. *Clays and Clay Minerals*, **39**, 387–399.
- Herbert J.-J., Kasbohm J., Moog H.C. & Henning, K.-J. (2004) Long-term behavior of the Wyoming bentonite MX-80 in high saline solutions. *Applied Clay Science*, **26**, 275–291.
- Hofmann U. & Klemen R. (1950) Verlust der Austauschfähigkeit von Lithiumionen an Bentonit durch Erhitzung. *Zeitschrift für Anorganische Chemie*, **262**, 95–99.
- Hofmann H., Bauer A. & Warr L.N. (2004) Behavior of smectite in strong salt brines under conditions relevant to the disposal of low- to medium-grade nuclear waste. *Clays and Clay Minerals*, **52**, 14–24.
- Holmes P.R. & Crundwell F.K. (2000) [The kinetics of the oxidation of pyrite by ferric ions and dissolved oxygen: an electrochemical study](#). *Geochimica et Cosmochimica Acta*, **64**, 263–274.
- Honty M., Uhlík P., Sucha V., Caploviová M., Francu J., Clauer N. & Biron A. (2004) Smectite-to-illite alteration in salt-bearing bentonites (the East Slovak basin). *Clays and Clay Minerals*, **52**, 533–551.
- Horváth I. & Novák I. (1976). Potassium fixation and the charge of montmorillonite layers. Pp. 185–189 in: *Proceedings of the International Clay Conference, Mexico City, 1975* (S.W. Bailey, editor). Applied Publishing, Wilmette, IL, USA.
- Hower J., Eslinger E.V., Hower M.E. & Perry Jr, E.A. (1976) Mechanism of burial metamorphism of argillaceous sediment, I. Mineralogical and chemical evidence. *Geological Society of America Bulletin*, **85**, 827.

- Huang W.-L., Longo J.M. & Pevear D.R. (1993) An experimentally derived kinetic model for smectite-to-illite conversion and its use as a geothermometer. *Clays and Clay Minerals*, **41**, 162–177.
- Hunger S. & Benning L.G. (2007) Greigite: a true intermediate on the polysulfide pathway to pyrite. *Geochemical Transactions*, **8**, 1–20.
- Inoue A. (1983) Potassium fixation by clay minerals during hydrothermal treatment. *Clays and Clay Minerals*, **31**, 81–91.
- Inoue A. (1984) Thermodynamic study of Na–K–Ca exchange reactions in Vermiculite. *Clays and Clay Minerals*, **32**, 311–319.
- Itälä A. & Muurinen A. (2012) Na/Ca selectivity coefficients of montmorillonite in perchlorate solution at different temperatures. *Materials Research Society Symposium Proceedings*, **1475**, 335–340.
- Jacques D., Phung Q.T., Perko J., Seetharam S.C., Maes N., Liu S. *et al.* (2021) Towards a scientific-based assessment of long-term durability and performance of cementitious materials for radioactive waste conditioning and disposal. *Journal of Nuclear Materials*, **557**, 32767–32767.
- Jaisi D.P., Kukkadapu R.K., Eberl D.D. & Dong H. (2005) Control of Fe(III) site occupancy on the rate and extent of microbial reduction of Fe(III) in nontronite. *Geochimica et Cosmochimica Acta*, **69**, 5429–5440.
- Jerz J.K. & Rimstidt J.D. (2004) Pyrite oxidation in moist air. *Geochimica et Cosmochimica Acta*, **68**, 701–714.
- Jodin-Caumon M.C., Mosser-Ruck R., Randi A., Pierron O., Cathelineau M. & Michau N. (2012) Mineralogical evolution of a claystone after reaction with iron under thermal gradient. *Clays and Clay Minerals*, **60**, 443–455.
- Johannesson L.-E., Börgesson L., Goudarzi R., Sandén T., Gunnarsson D. & Svemar C. (2007) Prototype repository: a full-scale experiment at Äspö HRL. *Physics and Chemistry of the Earth*, **32**, 58–76.
- Kale R.C. & Ravi K. (2018) Influence of thermal loading on index and physico-chemical properties of Barmer bentonite. *Applied Clay Science*, **165**, 22–39.
- Kappler A., Bryce C., Manson M., Lueder U., Byrne J.M. & Swanner E.D. (2021) An evolving view on biogeochemical cycling of iron. *Nature Reviews Microbiology*, **19**, 360–374.
- Karnland O. (1995) *Salt Redistribution and Enrichment in Compacted Bentonite Exposed to a Thermal Gradient*. SKB AR 95-31. Svensk Kärnbränslehantering AB, Stockholm, Sweden, 100 pp.
- Karnland O. & Birgersson M. (2006) *Montmorillonite Stability. With Special Respect to KBS-3 Conditions*. Swedish Nuclear Fuel and Waste Management Co., Technical Report TR-06-11. Svensk Kärnbränslehantering AB, Stockholm, Sweden, 38 pp.
- Karnland O., Olsson S., Dueck A., Birgersson M., Nilsson U., Hernan-Håkansson T. *et al.* (2009) *Long Term Test of Buffer Material at the Äspö Hard Rock Laboratory, LOT Project, Final Report on the A2 Test Parcel*. Technical Report TR-09-29. Svensk Kärnbränslehantering AB, Stockholm, Sweden, 279 pp.
- Kaufhold S. & Dohrmann R. (2010a) Effect of extensive drying on the cation exchange capacity of bentonites. *Clay Minerals*, **45**, 441–448.
- Kaufhold S. & Dohrmann R. (2010b) Stability of bentonites in salt solutions II. Potassium chloride solution – initial step of illitization? *Applied Clay Science*, **49**, 98–107.
- Kaufhold S. & Dohrmann R. (2013) The variable charge of dioctahedral clay minerals. *Journal of Colloid and Interface Science*, **390**, 225–233.
- Kaufhold S., Dohrmann R., Koch D. & Houben G. (2008) The pH of aqueous bentonite suspensions. *Clays and Clay Minerals*, **56**, 338–343.
- Kaufhold S., Stührenberg D. & Dohrmann R. (2009) Water redistribution between bentonite and halite at elevated temperature. *Applied Clay Science*, **46**, 245–250.
- Kaufhold S., Dohrmann R., Stucki J. & Anastácio A.S. (2011) Layer charge density of montmorillonite – closing the gap between structural formula method and alkyl ammonium method. *Clays and Clay Minerals*, **59**, 200–211.
- Kaufhold S., Dohrmann R., Sandén T., Sellin P. & Svensson D. (2013) Mineralogical investigations of the alternative buffer material test - I. Alteration of bentonites. *Clay Minerals*, **48**, 199–213.
- Kaufhold S., Sanders D., Dohrmann R. & Hassel A.-W. (2015) Fe corrosion in contact with bentonites. *Journal of Hazardous Materials*, **285**, 464–473.
- Kaufhold S., Dohrmann R. & Ufer K. (2016) Interaction of magnesium cations with dioctahedral smectites under HLRW repository conditions. *Clays and Clay Minerals*, **64**, 743–752.
- Kaufhold S., Dohrmann R., Götze N. & Svensson D. (2017) Characterisation of the second parcel of the alternative buffer material (ABM) experiment – I. Mineralogical reactions. *Clays and Clay Minerals*, **65**, 27–41.
- Kaufhold S., Dohrmann R., Ufer K. & Kober F. (2018) Interactions of bentonite with metal and concrete from the FEBEX experiment – mineralogical and geochemical investigations of selected sampling sites. *Clay Minerals*, **53**, 745–763.
- Kaufhold S., Dohrmann R., Degtjarev A., Koeniger P. & Post V. (2019) Mg and silica release in short-term dissolution tests in bentonites. *Applied Clay Science*, **172**, 106–114.
- Kaufhold S., Dohrmann R. & Ufer K. (2020a) Determining the extent of bentonite alteration at the bentonite/cement interface. *Applied Clay Science*, **186**, 105446.
- Kaufhold S., Klimke S., Schlömer S., Alpermann T., Renz F. & Dohrmann R. (2020b) About the corrosion mechanism of metal iron in contact with bentonite. *Earth and Space Chemistry*, **4**, 711–721.
- Kaufhold S., Dohrmann R., Ufer K., Svensson D. & Sellin P. (2021) Mineralogical analysis of bentonite from the ABM5 heater experiment at Äspö Hard Rock Laboratory, Sweden. *Minerals*, **11**, 669.
- Kohfahl C. & Pekdeger A. (2006) Rising groundwater tables in partly oxidized pyrite bearing dump-sediments: column study and modelling approach. *Journal of Hydrology*, **331**, 703–718.
- Kuligiewicz A. & Derkowski A. (2017) Tightly bound water in smectites. *American Mineralogist*, **102**, 1079–1090.
- Kumpulainen S., Kiviranta L. & Korkeakoski P. (2016) Long-term effects of Fe-heater and Äspö groundwater on smectite clays – chemical and hydro-mechanical results from *in situ* Alternative Buffer Material (ABM) test package 2. *Clay Minerals*, **51**, 129–144.
- Kyllönen J., Hakanen M., Lindberg A., Harjula R., Vehkamäki M. & Lehto J. (2014) Modeling of cesium sorption on biotite using cation exchange selectivity coefficients. *Radiochimica Acta*, **102**, 919–929.
- Lagaly G. (1993) *Reaktionen der Tonminerale*. Pp. 89–167 in: *Tonminerale und Tone* (K. Jasmund & G. Lagaly, editors). Steinkopff Verlag, Darmstadt, Germany.
- Lanson B., Lantenois S., van Aken P.A., Bauer A. & Plançon A. (2012) Experimental investigation of smectite interaction with metal iron at 80°C: structural characterization of newly formed Fe-rich phyllosilicates. *American Mineralogist*, **97**, 864–871.
- Lantenois S., Lanson B., Muller F., Bauer A., Jullien M. & Plançon A. (2005) Experimental study of smectite interaction with metal Fe at low temperature: I. Smectite destabilization. *Clays and Clay Minerals*, **53**, 597–612.
- Larsen O. & Postma D. (2001) Kinetics of reductive bulk dissolution of lepidocrocite, ferrihydrite, and goethite. *Geochimica et Cosmochimica Acta*, **65**, 1367–1379.
- Lasaga A.C. (1998) *Kinetic Theory in the Earth Sciences*. Princeton University Press, Princeton, NJ, USA, 811 pp.
- Lefebvre R., Hockley D., Smolensky J. & Gélinas P. (2001) Multiphase transfer processes in waste rock piles producing acid mine drainage: I: conceptual model and system characterization. *Journal of Contaminant Hydrology*, **52**, 137–164.
- Lippmann F. (1979) Stabilitätsbeziehungen der Tonminerale, stability relations of clay minerals. *Neues Jahrbuch für Mineralogie*, **136**, 287–309.
- Liu C.X., Zachara J.M. & Smith S.C. (2004) A cation exchange model to describe Cs⁺ sorption at high ionic strength in subsurface sediments at Hanford site, USA. *Journal of Contaminant Hydrology*, **68**, 217–238.
- Lu C., Samper J., Fritz B., Clement A. & Montenegro L. (2011) Interactions of corrosion products and bentonite: an extended multicomponent reactive transport model. *Physics and Chemistry of the Earth Parts A/B/C*, **36**, 1661–1668.
- Mackenzie R.C. (1963) Retention of exchangeable ions by montmorillonite. Pp. 183–193 in: *International Clay Conference 1963* (I.T. Rosenquist & P. Graff-Petersen, editors). Pergamon Press, Oxford, UK.
- Maes A. & Cremers A. (1981) Cation exchange in clay minerals: some recent developments. Pp. 205–232 in: *Soil Chemistry B. Physico-Chemical Models*, 2nd edition (G.H. Bolt, editor), Vol. 5, part B of *Developments in Soil Science*. Elsevier, Amsterdam, The Netherlands.
- Maher K., Johnson N., Jackson A., Lammers L., Torchinsky A., Weaver K., Bird D. & Brown G. (2016) A spatially resolved surface kinetic model for forsterite dissolution. *Geochimica et Cosmochimica Acta*, **174**, 313–334.

- Martin F.A., Bataillone C. & Schlegel M.L. (2008) Corrosion of iron and low alloyed steel within a water saturated brick of clay under anaerobic deep geological disposal conditions: an integrated experiment. *Journal of Nuclear Materials*, **379**, 80–90.
- Martinez V., Abós H. & García-Siñeriz J.L. (2016) *FEDEXe AITEMIN Final Sensor Data Report (FEDEX 'In Situ' Experiment)*. Nagra Arbeitsbereich NAB 16-19. Nagra Arbeitsbereich, Wettingen, Switzerland, 244 pp.
- Marty N.C.M., Fritz B., Clément A. & Michau N. (2010) Modelling the long term alteration of the engineered bentonite barrier in an underground radioactive waste repository. *Applied Clay Science*, **47**, 82–90.
- Marty N.C.M., Claret F., Lassin A., Tremosa J., Blanc P., Madé B. et al. (2015) A database of dissolution and precipitation rates for clay-rocks minerals. *Applied Geochemistry*, **55**, 108–118.
- May H.M., Kinniburgh D.G., Helmke P.A. & Jackson M.L. (1986) Aqueous dissolution, solubilities and thermodynamic stabilities of common aluminosilicate clay minerals; kaolinite and smectite. *Geochimica et Cosmochimica Acta*, **50**, 1667–1677.
- Mazurek M., Alt-Epping P., Bath A., Gimmi T., Waber H.N., Buschaert S., De Cannière P., De Craen M., Gautschi A., Savoye S., Vinsot A., Wemaere I. & Wouters L. (2011) Natural tracer profiles across argillaceous formations. *Applied Geochemistry*, **26**, 1035–1064.
- McBride M.B. (1994) *Environmental Chemistry of Soils*. Oxford University Press, Oxford, UK, 416 pp.
- Mendili Y.E., Abdeloual Ait A., Chaou A., Bardeau J.-F. & Schlegel M.L. (2014) Carbon steel corrosion in clay-rich environment. *Corrosion Science*, **88**, 56–65.
- Meunier A. & Velde B. (2004) *Illite: Origins, Evolution, and Metamorphism*. Springer, Berlin, Germany, 286 pp.
- Missana T., Benedicto A., García-Gutiérrez M. & Alonso U. (2014) Modeling cesium retention onto Na-, K- and Ca-smectite: effects of ionic strength, exchange and competing cations on the determination of selectivity coefficients. *Geochimica et Cosmochimica Acta*, **128**, 266–277.
- Montes H.G., Marty N., Fritz B., Clément A. & Michau N. (2005) Modelling of long-term diffusion – reaction in a bentonite barrier for radioactive waste confinement. *Applied Clay Science*, **30**, 181–198.
- Moses C.O., Nordstrom K., Herman J.S. & Mills A.L. (1987) Aqueous pyrite oxidation by dissolved oxygen and by ferric iron. *Geochimica et Cosmochimica Acta*, **51**, 1561–1571.
- Mota-Heredia C., Cuevas J., Ruiz A.I., Ortega A., Torres E., Turrero M.J. & Fernández R. (2023) Geochemical interactions at the steel–bentonite interface caused by a hydrothermal gradient. *Applied Clay Science*, **240**, 106984.
- Müller-Vonmoos M., Kahr G., Bucher F. & Madsen F. (1990) Investigation of Kinnekulle K-bentonite aimed at assessing the long-term stability of bentonites under repository conditions. *Engineering Geology*, **28**, 269–280.
- Müller-Vonmoos M., Kahr G. & Madsen F. (1994) Intracrystalline swelling of mixed-layer illite–smectite in K-bentonites. *Clay Minerals*, **29**, 205–213.
- Muurinen A. (2006) *Chemical Conditions in the A2 Parcel of the Long-Term Test of Buffer Material in Äspö (LOT)*. Working Report 2006-83. Posiva Oy, Olkiluoto, Finland, 28 pp.
- Neretnieks I. (1978) *Transport of Oxidants and Radionuclides through a Clay Barrier*. Kungl Tekniska Högskolan Stockholm 1978-02-20. Kungl Tekniska Högskolan, Stockholm, Sweden, 45 pp.
- Newton R.C. & Manning C.E. (2005) Solubility of Anhydrite, CaSO₄, in NaCl–H₂O solutions at high pressures and temperatures: applications to fluid–rock interaction. *Journal of Petrology*, **46**, 701–716.
- Ngo V.V., Delalande M., Clément A., Michau N. & Fritz B. (2014). Coupled transport–reaction modeling of the long-term interaction between iron, bentonite and Callovo-Oxfordian claystone in radioactive waste confinement systems. *Applied Clay Science*, **101**, 430–443.
- Nordstrom D.K. (2011) *Mine waters: acidic to circumneutral*. *Elements*, **7**, 393–398.
- Nordstrom D.K. (2013) Improving internal consistency of standard state thermodynamic data for sulfate ion, portlandite, gypsum, barite, celestine, and associated ions. *Procedia Earth and Planetary Science*, **7**, 624–627.
- Nordstrom D.K. & Southam G. (1997). Geomicrobiology of sulfide mineral oxidation. *Geomicrobiology: Interactions Between Microbes and Minerals*, **35**, 361–390.
- Nordstrom D.K., Plummer L.N., Langmuir D., Busenberg E., May H.M., Jones B.F. & Parkhurst D.L. (1990) Revised chemical equilibrium data for major water–mineral reactions and their limitations. Pp. 398–413 in: *Chemical Modeling of Aqueous Systems II* (D.C. Melchior & R.L. Bassett, editors). American Chemical Society, Washington, DC, USA.
- Oda C., Honda A. & Savage D. (2004) An Analysis of Cement–Bentonite Interaction and Evolution of Pore Water Chemistry. Pp. 74–79 in: *Proceedings of the International Workshop on Bentonite–Cement Interaction in Repository Environments* (R. Metcalfe & C. Walker, editors). Nuclear Waste Management Organization of Japan, Tokyo, Japan.
- Olsson S., Jensen V., Johannesson L.-E., Hansen E., Karnland O., Kumpulainen S. et al. (2013) *Prototype Repository. Hydromechanical, Chemical and Mineralogical Characterization of the Buffer and Backfill Material from the Outer Section of the Prototype Repository*. SKB TR-13-21. Svensk Kärnbränslehantering AB, Stockholm, Sweden, 163 pp.
- Osacky M., Šucha V.A., Czimerová A. & Madejová J. (2010) Reaction of smectites with iron in a nitrogen atmosphere at 75°C. *Applied Clay Science*, **50**, 237–244.
- Parkhurst D.L. & Appelo C.A.J. (1999) *User's Guide to PHREEQC (Version 2)*. US Geological Survey, Denver, CO, USA, 327 pp.
- Parkhurst D.L. & Appelo C.A.J. (2013) *Description of Input and Examples for PHREEQC Version 3 – A Computer Program for Speciation, Batch-Reaction, One-Dimensional Transport, and Inverse Geochemical Calculations*. US Geological Survey, Denver, CO, USA, 519 pp.
- Parry S.A., Hodson M.E., Kemp S.J. & Oelkers E.H. (2015) The surface area and reactivity of granitic soils: I. Dissolution rates of primary minerals as a function of depth and age deduced from field observations. *Geoderma*, **237–238**, 21–35.
- Perronnet M., Villières F., Jullien M., Razafitianamaharavo A., Raynal J. & Bonnin D. (2007) Towards a link between the energetic heterogeneities of the edge faces of smectites and their stability in the context of metallic corrosion. *Geochimica et Cosmochimica Acta*, **71**, 1463–1479.
- Plötze M., Kahr G., Dohrmann R. & Weber H. (2007) Hydro-mechanical, geochemical and mineralogical characteristics of the bentonite buffer in a heater experiment. The HE-B project at the Mont Terri rock laboratory. *Physics and Chemistry of the Earth*, **32**, 730–740.
- Prommer H. & Stuyfzand P.J. (2005) Identification of temperature-dependent water quality changes during a deep well injection experiment in a pyritic aquifer. *Environmental Science & Technology*, **39**, 2200–2209.
- Psenner R. (1983) Die Entstehung von Pyrit in rezenten Sedimenten des Piburger Sees. *Schweizerische Zeitschrift für Hydrologie*, **45**, 219–232.
- Pusch R. (1983) *Stability of Deep-Sited Smectite Minerals in Crystalline Rock-Chemical Aspects*. KBS 83 16. Swedish Nuclear Fuel and Waste Management Company, Stockholm, Sweden, 103 pp.
- Pye K. & Miller J.A. (1990) Chemical and biochemical weathering of pyritic mudrocks in a shale embankment. *Quarterly Journal of Engineering Geology and Hydrogeology*, **23**, 365–382.
- Pytte A.M. (1982) *The Kinetics of Smectite to Illite Reaction in Contact Metamorphic Shales*. MA thesis, Dartmouth College, Hanover, NH, USA.
- Pytte A.M. & Reynolds R. C. (1989) The thermal transformation of smectite to illite. Pp. 133–140 in: *Thermal history of Sedimentary Basins* (N.D. Naeser & T.H. McCulloh, editors). Springer-Verlag, New York, NY, USA.
- Reiss A.G., Gavrieli I., Rosenberg Y.O., Reznik I.J., Luttge A., Emmanuel S. & Ganor J. (2021) Gypsum precipitation under saline conditions: thermodynamics, kinetics, morphology, and size distribution. *Minerals*, **11**, 141.
- Rimstidt J.D. & Barnes H.L. (1980) The kinetics of silica–water reactions. *Geochimica et Cosmochimica Acta*, **44**, 1683–1699.
- Rimstidt D.D. & Vaughan D.J. (2003) Pyrite oxidation: a state-of-the-art assessment of the reaction mechanism. *Geochimica et Cosmochimica Acta*, **67**, 873–880.
- Romaine A., Sabot R., Jeannin, M. & Refait P. (2013) Electrochemical synthesis and characterization of corrosion products on carbon steel under argillite layers in carbonated media at 80°C. *Electrochimica Acta*, **114**, 152–158.
- Rozalén M.L., Huertas F.J., Brady P.V., Cama J., Garcia-Palma S. & Linares J. (2008) Experimental study of the effect of pH on the kinetics of montmorillonite dissolution at 25°C. *Geochimica et Cosmochimica Acta*, **72**, 4224–4253.
- Ruiz-Agudo E., Putnis C.V., Hövelmann J., Álvarez-Lloret P., Ibáñez-Velasco A. & Putnis A. (2015) Experimental study of the replacement of calcite by calcium sulphates. *Geochimica et Cosmochimica Acta*, **156**, 75–93.

- Saheb M., Descostes M., Neff D., Matthiesen H., Michelin A. & Dillmann P. (2010) Iron corrosion in an anoxic soil: Comparison between thermodynamic modelling and ferrous archaeological artefacts characterised along with the local in situ geochemical conditions. *Applied Geochemistry*, **25**, 1937–1948.
- Saheb M., Neff D., Demory J., Foy E. & Dillmann P. (2013) Characterisation of corrosion layers formed on ferrous archaeological artefacts buried in anoxic media. *Corrosion Engineering, Science and Technology*, **45**, 381–387.
- Samper J., Lu C. & Montenegro L. (2008). Reactive transport model of interactions of corrosion products and bentonite. *Physics and Chemistry of the Earth Parts A/B/C*, **33**, 306–316.
- Samper J., Naves A., Montenegro L. & Mon A. (2016) Reactive transport modelling of the long-term interactions of corrosion products and compacted bentonite in a HLW repository in granite: uncertainties and relevance for performance assessment. *Applied Geochemistry*, **67**, 42–51.
- Samper J., Mon A. & Montenegro L. (2018) A revisited thermal, hydrodynamic, chemical and mechanical model of compacted bentonite for the entire duration of the FEBEX *in situ* test. *Applied Clay Science*, **160**, 58–70.
- Sauer K., Caporuscio F., Rock M., Cheshire M. & Jové-Colón C. (2020) Hydrothermal interaction of Wyoming bentonite and Opalinus clay. *Clays and Clay Minerals*, **68**, 144–160.
- Savage D., Walker C., Arthur R., Rochelle C., Oda C. & Takase H. (2007) Alteration of bentonite by hyperalkaline fluids: a review of the role of secondary minerals. *Physics and Chemistry of the Earth Parts A/B/C*, **32**, 287–297.
- Savage D., Watson C., Benbow S. & Wilson J. (2010) Modelling iron–bentonite interactions. *Applied Clay Science*, **47**, 91–98.
- Savage D., Wilson J., Benbow S., Sasamoto H., Oda C., Walker C., Kawama D. & Tachi Y. (2020) Using natural systems evidence to test models of transformation of montmorillonite. *Applied Clay Science*, **195**, 105741.
- Savoye S., Legrand L., Sagon G., Lecomte S., Chausse A., Messina R. & Toulhoata P. (2001) Experimental investigations on iron corrosion products formed in bicarbonate/carbonate-containing solutions at 90°C. *Corrosion Science*, **43**, 2049–2064.
- Sawaguchi T., Tsukada M., Yamaguchi T. & Mukai M. (2016) Effects of OH⁻ activity and temperature on the dissolution rate of compacted montmorillonite under highly alkaline conditions. *Clay Minerals*, **51**, 267–278.
- Schlosser J., Grathoff G., Warr L., Derkowski A., Kaufhold S., Schleicher A.M. & Wirth R. (2019) *The influence of K-bearing organic acids on the alteration of smectite: new experimental results*. Presented at: Euroclay 2019, Paris, France, 1–5 July.
- Sellin P. & Leupin O.X. (2013) The use of clay as an engineered barrier in radioactive waste management – a review. *Clays and Clay Minerals*, **61**, 477–498.
- Sena C., Salas J., & Arcos D. (2010) *Thermo-hydro-geochemical Modelling of the Bentonite Buffer LOT A2 Experiment*. Swedish Nuclear Fuel and Waste Management Co, Technical Report, TR-10-65. Swedish Nuclear Fuel and Waste Management Company, Stockholm, Sweden, 53 pp.
- Shen L., Sippola H., Li X., Lindberg D. & Taskinen R. (2019) Thermodynamic Modelling of Calcium Sulfate Hydrates in the CaSO₄–H₂O System from 273.15 to 473.15 K with Extension to 548.15 K. *Journal of Chemical Engineering Data*, **64**, 2697–2709.
- Smart N.R., Reddy B., Rance A.P., Nixon D.J., Frutschi M., Bernier-Latmani R. & Diomidis N. (2017) The anaerobic corrosion of carbon steel in compacted bentonite exposed to natural Opalinus Clay porewater containing native microbial populations. *International Journal of Corrosion Processes and Corrosion Control*, **52**, 101–112.
- Stoullil J., Kanok J., Kouril M., Parschova, H. & Novak P. (2013) Influence of temperature on corrosion rate and porosity of corrosion products of carbon steel in anoxic bentonite environment. *Journal of Nuclear Material*, **443**, 20–25.
- Suzuki S., Sazarashi M., Akimoto T., Haginuma M. & Suzuki K. (2008) A study of the mineralogical alteration of bentonites in saline water. *Applied Clay Science*, **41**, 190–198.
- Svensson D. (2015) Saponite formation in the ABM2 ironbentonite field experiment at Äspö hard rock laboratory, Sweden. Pp. 168–169 in: *Clays in Natural and Engineered Barriers for Radioactive Waste Confinement, Sixth International Meeting, Program & Abstracts*. Agence nationale pour la gestion des déchets radioactifs, Paris, France.
- Svensson P.D. & Hansen S. (2013) Redox chemistry in two iron-bentonite field experiments at Äspö hard rock laboratory, Sweden: an XRD and Fe K-edge XANES study. *Clays and Clay Minerals*, **61**, 566–579.
- Svensson D., Dueck A., Nilsson U., Olsson S., Sandén T., Lydmark S. *et al.* (2011) *Alternative Buffer Material. Status of the Ongoing Laboratory Investigation of Reference Materials and Test Package 1*. TR-11-06. Svensk Kärnbränslehantering AB, Stockholm, Sweden, 140 pp.
- Tournassat C., Gailhanou H., Crouzet C., Braibant G., Gautier A., Lassin, A. *et al.* (2007) Two cation exchange models for direct and inverse modelling of solution major cation composition in equilibrium with illite surfaces. *Geochimica et Cosmochimica Acta*, **71**, 1098–1114.
- Udo E.J. (1978) Thermodynamics of potassium–calcium and magnesium–calcium exchange reactions on a kaolinite soil clay. *Soil Science Society of America Journal*, **42**, 556–560.
- Uzarowicz L. & Skiba S. (2011) Technogenic soils developed on mine spoils containing iron sulphides: mineral transformations as an indicator of pedogenesis. *Geoderma*, **163**, 95–108.
- Velde B. & Vasseur G. (1992) Estimation of the diagenetic smectite to illite transformation in time temperature space. *American Mineralogist*, **77**, 967–976.
- Verron H., Sterpenich J., Bonnet J., Bourdelle F., Mosser-Ruck R., Lorgeoux C. *et al.* (2019) Experimental study of pyrite oxidation at 100°C: implications for deep geological radwaste repository in claystone. *Minerals*, **9**, 427.
- Vogt K. & Köster H.M. (1978) Zur Mineralogie, Kristallchemie und Geochemie einiger Montmorillonite aus Bentoniten. *Clay Minerals*, **13**, 25–43
- Voigt M., Marieni C., Deirdre E.C., Gislason S.R. & Oelkers E.H. (2018) Evaluation and refinement of thermodynamic databases for mineral carbonation. *Energy Procedia*, **146**, 81–91.
- Wallis I. & Pichler T. (2018) [Generating false negatives and false positives for As and Mo concentrations in groundwater due to well installation](#). *Science of the Total Environment*, **631–632**, 723–732.
- Wallis I., Idiart A., Dohrmann R. & Post V. (2016) Reactive transport modelling of groundwater-bentonite interaction: effects on exchangeable cations in an alternative buffer material in-situ test. *Applied Geochemistry*, **73**, 59–69.
- Weiss A. & Koch G. (1961). Über einen Zusammenhang zwischen dem Verlust des innerkristallinen Quellungsvermögens beim Erhitzen und dem Schichtaufbau bei glimmerartigen Schichtsilikaten. *Zeitschrift für Naturforschung*, **16B**, 68–69.
- Wersin P., Jenni A. & Maeder U. (2013) Interaction of corroding iron with bentonite at repository conditions. Goldschmidt abstracts. *Mineralogical Magazine*, **77**, 2482.
- White A.F. & Brantley S.L. (2003) The effect of time on the weathering of silicate minerals: why do weathering rates differ in the laboratory and field? *Chemical Geology*, **202**, 479–506.
- White A.F. & Peterson M.L. (1990) Role of reactive-surface-area characterization in geochemical kinetic models. Pp. 461–475 in: *Chemical Modeling of Aqueous Systems II* (D.C. Melchior & R.L. Bassett, editors). American Chemical Society, Washington, DC, USA.
- Wieland E., Mäder U., Lothenbach B., Jenni A. & Bernard E. (2017) Editorial – mechanisms and modelling of waste-cement and cement–host rock interactions. *Physics and Chemistry of the Earth Parts A/B/C*, **99**, 1–2.
- Williamson M.A. & Rimstidt J.D.D. (1994) The kinetics and electrochemical rate-determining step of aqueous pyrite oxidation. *Geochimica et Cosmochimica Acta*, **58**, 5443–5454.
- Wilson J.C., Cressey G., Cressey B., Cuadros J., Ragnarsdottir K.V., Savage D. & Shibata M. (2006a) The effect of iron on montmorillonite stability. (II) Experimental investigation. *Geochimica et Cosmochimica Acta*, **70**, 323–336.
- Wilson J.C., Savage D., Cuadros J., Shibata M. & Ragnarsdottir K.V. (2006b) The effect of iron on the montmorillonite stability. (I) Background and thermodynamic considerations. *Geochimica et Cosmochimica Acta*, **70**, 306–322.
- Wilson J.C., Benbow S., Sasamoto H., Savage D. & Watson C. (2015) Thermodynamic and fully-coupled reactive transport models of a steel–bentonite interface. *Applied Geochemistry*, **61**, 10–28.

- Xie X., Xiao S., He Z., Liu J. & Qiu G. (2007) Microbial populations in acid mineral bioleaching systems of Tong Shankou Copper Mine, China. *Journal of Applied Microbiology*, **103**, 1227–1238.
- Xu T., Senger R. & Finsterle S. (2008) Corrosion-induced gas generation in a nuclear waste repository: reactive geochemistry and multiphase flow effects. *Applied Geochemistry*, **23**, 3423–3433.
- Yi X., Su D., Seigneur N. & Mayer K.U. (2021) Modeling of thermal-hydrological-chemical (THC) processes during waste rock weathering under permafrost conditions. *Frontiers in Water*, **3**, 645675.
- Yokoyama S., Shimbashi M., Minato D., Watanabe Y., Jenni A. & Mäder U. (2021) Alteration of bentonite reacted with cementitious materials for 5 and 10 years in the Mont Terri rock laboratory (CI experiment). *Minerals*, **11**, 251.
- Zandanel A., Sauer K.B., Rock M., Caporuscio F.A., Telfeyan K. & Matteo E.N. (2022) Impacts of crystalline host rock on repository barrier materials at 250 °C: hydrothermal co-alteration of Wyoming bentonite and steel in the presence of Grimsel granodiorite. *Minerals*, **12**, 1556.
- Zheng L., Rutqvist J., Birkholzer J.T. & Liu H.-H. (2015) On the impact of temperatures up to 200 °C in clay repositories with bentonite engineer barrier systems: a study with coupled thermal, hydrological, chemical, and mechanical modelling. *Engineering Geology*, **197**, 278–295.
- Zheng L., Rutqvist J., Xu H. & Birkholzer J.T. (2017) Coupled THMC models for bentonite in an argillite repository for nuclear waste: illitization and its effect on swelling stress under high temperature. *Engineering Geology*, **230**, 118–129.